3 Growth and Surface Properties of Apatite

John Rakovan

Department of Geology
Miami University
Oxford, Ohio 45056

INTRODUCTION

The surface defines the interface between a mineral and its surroundings. In a dynamic context, reactions that occur between apatites and the environments in which they exist take place at or through their surfaces. This includes, but is not restricted to, crystal growth, dissolution, and surface-mediated reactions such as sorption, surface complexation, and catalysis (Hochella and White 1990). Because this interface is partly defined by the nature of the environment around the crystal, the properties, structure and chemistry of the crystal surface are always different than those of the bulk, and can be quite varied depending on the environment. For example, the crystal surface of apatite may have very different characteristics in contact with an aqueous solution as opposed to a polymerized silicate melt.

Understanding the behavior of apatite surfaces is important on both the local and global scale. Apatite-water interactions can influence global biogeochemical systems such as the phosphorus cycle and the fate and transport of trace elements in Earth surface environments. The rapidly growing integration of surface science with the geological sciences is due to the realization that mineral surfaces are of great importance in a wide variety of natural processes. In order to understand the role of mineral surfaces on a global scale we must first understand the details of their structure and the interactions that take place on those surfaces at the atomic scale. This chapter provides a review of the nature of the apatite surface, particularly as it exists in contact with aqueous solutions, and the processes involved in apatite crystal growth.

CRYSTAL MORPHOLOGY AND SURFACE MICROTOPOGRAPHY

Morphology

In igneous, metamorphic and hydrothermal systems apatite is most often found as euhedral to subhedral hexagonal crystals. The habit is usually prismatic, elongate along [001], or tabular, although equant crystals are not uncommon (Fig. 1). The most common forms are {100}, {001}, {101}, and {110}. However, the combination of many other forms can lead to complex morphologies. Goldschmidt (1913) provides 13 pages of crystal drawings exhibiting more than 17 distinct forms. Palache et al. (1951) list 30 forms that have been observed on apatite. Although many apatite crystals are only bound by two forms, {001} and {100}, some crystals are very complex, with six or more forms on a single crystal (Fig. 2). Crystals are also found as anhedral massive, granular or globular. Sedimentary apatites are most often found as massive, cryptocrystalline crusts, concretions, stalactites and masses of radiating fibers, collectively known as collophane.

Much is known about the causes of morphologic variations in crystals (Kostov and Kostov 1999, Sunagawa 1987a); however, little has been done to investigate the factors that control apatite crystal morphology specifically. In a study of the affect of fluorine concentration in solution on the morphology and growth rate of fluorapatite, Deutsch and Sarig (1977) found that at high fluorine concentrations (F concentrations in excess of 4× the stoichiometric amount for fluorapatite) the crystal habit was found to be

1529-6466/03/0048-0003$05.00 DOI: 10.2138/rmg.2002.48.3

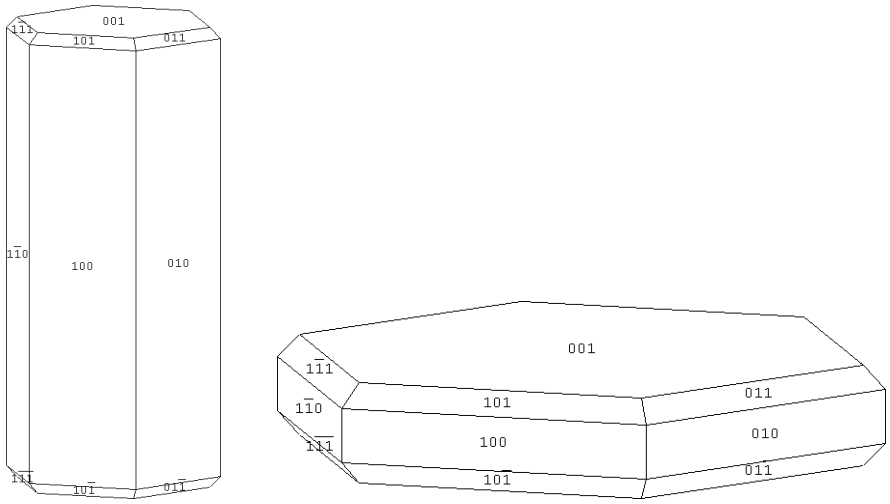

Figure 1. Depictions of prismatic and tabular apatite crystals.

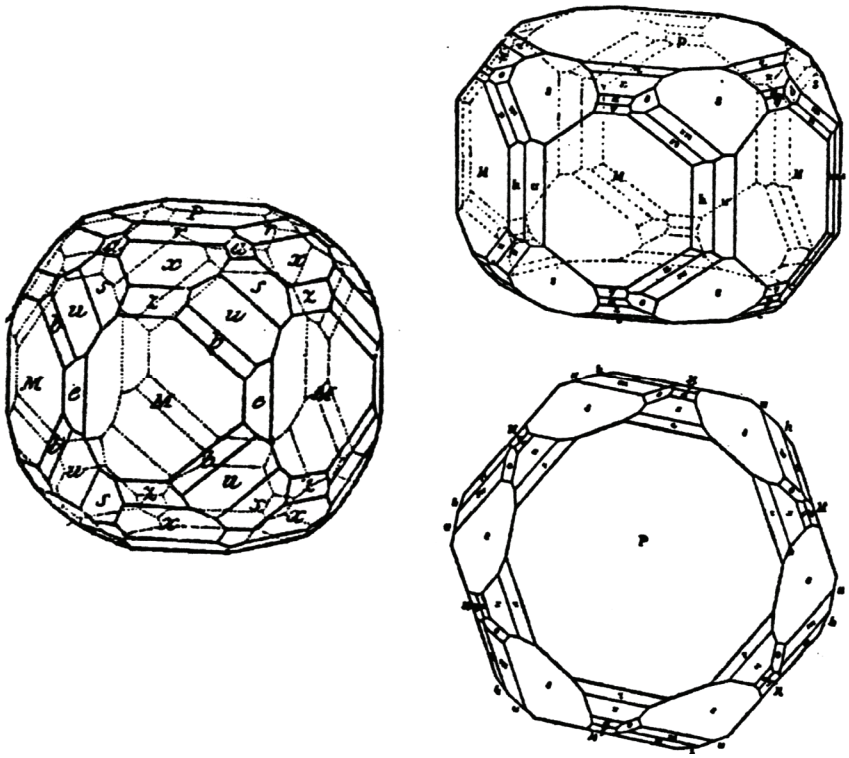

Figure 2. Depictions of complex apatite crystals. [Modified after Goldschmidt (1913).]

tabular, whereas at low fluorine concentrations (F concentrations less than 4× the stoichiometric amount for fluorapatite) the habit was needle-like.

Biological apatite in bone and teeth often has a distinct morphology, unlike any inorganic apatites. Individual crystals are usually platy or ribbon-like (Nylen et al. 1963, Christoffersen and Landis 1991), with rectangular cross sections (Fig. 3). It has been suggested that these form as pseudomorphs of a precursor phase such as octacalcium phosphate, OCP (Brown 1966). OCP forms thin, bladed crystals that are dominated by the {100} form and elongate in [001] (Terpstra and Bennema 1987). Some biological apatites, however, show a hexagonal morphology (Fig. 4; Nylen et al. 1963). The existence of precursor phases in the growth of apatite is discussed in detail later.

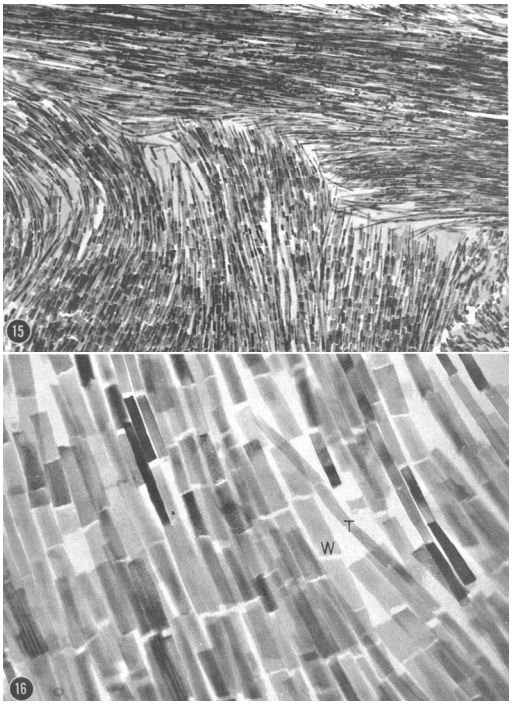

Figure 3. TEM photomicrographs of hydroxyl-apatite from rat bone. The direction of crystal elongation is [001]. Magnification is 35,000× and 150,000× in the upper and lower images respectively. [Used by permission of The Rockefeller University Press, from Nylen et al. (1963) *Journal of Cell Biology*, Vol. 18, Figs. 15 & 16, p. 119.]

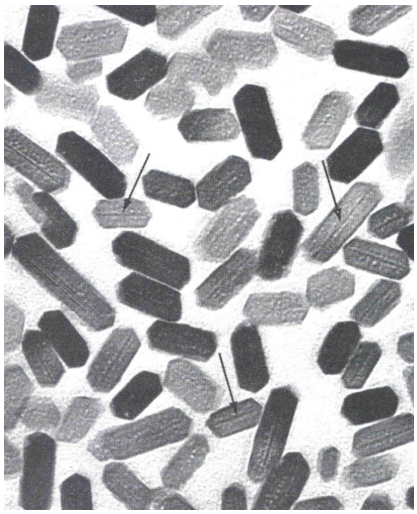

Figure 4. TEM photomicrograph of hydroxylapatite from rat bone. Crystals are oriented with {001} parallel to the image plane. Magnification is 300,000x. [Used by permission of The Rockefeller University Press, from Nylen et al. (1963) Jour. Cell Biology, Vol. 18, Fig. 13, p. 117.]

Apatites range in size from submicron crystals, like those found in biological systems, to giant metamorphic crystals weighing many tons. Velthuizen (1992) and Hogarth (1974) summarize reports of large crystals from Grenville province metasediments including "a solid but irregular mass of green crystalline apatite, 15 feet long and 9 feet wide" and a single euhedral crystal from the Aetna mine measuring 2.1 × 1.2 m with an estimated weight of 6 tons.

Surface microtopography

The microtopography of apatite crystal surfaces can vary greatly depending on the crystal face observed, conditions of crystal growth and growth mechanism, the degree and type of physical abrasion, cleavage or fracture, and the degree and mechanism of dissolution. The scale of microtopographic features on crystal surfaces ranges from atomic dimensions to dimensions of the entire crystal. Surface microtopographic features observed *ex situ* are often important clues to the conditions in, and mechanisms by, which crystals have formed, as well as post-growth reactions with the environment (Sunagawa 1987b). Thus, surface microtopography can be powerful for the interpretation of the growth and weathering history of apatite.

Growth. For crystal growth processes, one microtopographic feature that is unambiguously indicative of growth mechanism is a growth spiral (Burton et al. 1951, Sunagawa 1984, Sunagawa 1987b). Under conducive growth conditions (temperatures below the roughening transition and relatively low supersaturation) spirals may be highly polygonized. Amelinckx (1952a) observed growth spirals of several different morphologies on the {100} faces of apatite crystals from Mexico. The exact location is not given, but from the description of the samples it is likely that they were from the deposits of Cerro del Mercado, Durango. The spirals indicate that growth was by the spiral mechanism (see section on growth mechanisms). Growth steps on the observed spirals were measured by reflected light techniques to be 10 ± 2 Å, which is, within error, the unit cell dimension normal to {100}. Crystals from Sulzbachtal, Austria also exhibit well-developed polygonized spirals on {100} faces, indicating growth by the spiral mechanism (Fig. 5) (Amelinckx 1952b). Apatites from both locations most likely grew from aqueous solutions (Amelinckx 1952b).

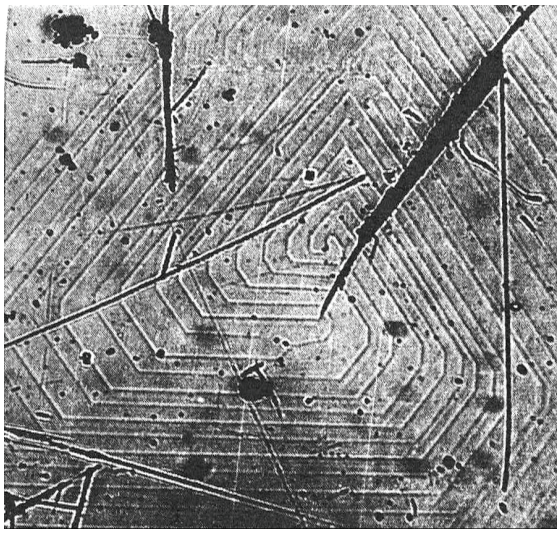

Figure 5. Reflected light photomicrograph of a complex growth spiral on a {100} face of an apatite crystal from Sulzbachtal, Austria. The horizontal steps run in the [001] direction. [Used by permission of Macmillan Publishers Ltd., from Amelinckx (1952) *Nature*, Vol. 170, Fig. 1, p. 760.]

Growth spirals can cause low mounds or growth hillocks to form on otherwise macroscopically flat crystal faces (Sunagawa 1987b, Reeder and Rakovan 1999, Paquette and Reeder 1995, Teng et al. 1999, Pina et al. 1998). If the growth spiral is polygonized, well-defined vicinal faces may be observed on the hillock (Müller-Krumbhaar et al. 1977, Sunagawa and Bennema 1982). Vicinal faces are shallow (usually only hundredths of one degree in inclination from the crystal faces on which they form), non-rational surfaces that are formed from multiple steps of like orientation that propagate in the same direction as adatoms or growth units are added to them during crystal growth. Growth hillocks have been observed on multiple forms of apatite. Rakovan and Reeder (1994) reported growth hillocks on {100} and {001} faces of hydrothermally precipitated apatites from numerous locations. They observed three-sided hillocks on {100} faces (Fig. 6a). The vicinal faces of these hillocks are made up steps that strike parallel to [001], [011], and $[01\bar{1}]$. The face symmetry of {100} is a mirror plane perpendicular to [001]. This mirror equates [011] and $[01\bar{1}]$ steps, however the [001] steps of the third vicinal face are symmetrically nonequivalent (Fig. 6b). These step orientations are parallel to the orientations of the dominant steps of growth spirals reported by Amelinckx (1952b). The majority of {100} faces on well-developed apatite crystals that form from aqueous solutions are striated with steps that strike along [001] only. However, three-sided hillocks on {100} faces, similar to those in Figure 6, are not uncommon and have been observed on apatites from pegmatite pockets, veins and other hydrothermal deposits from dozens of locations (personal observation). The {001} faces of apatites often exhibit

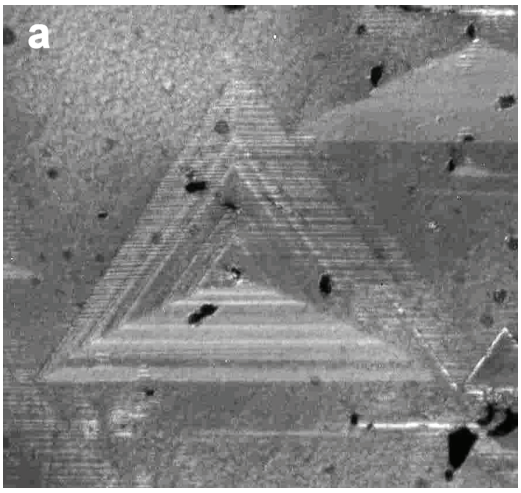

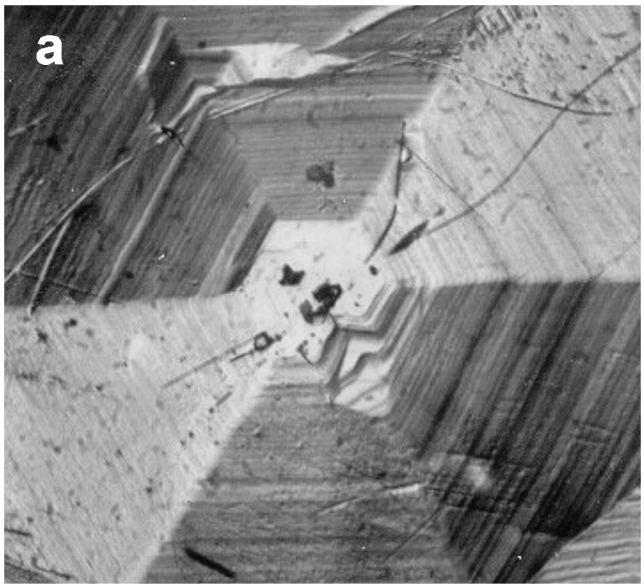

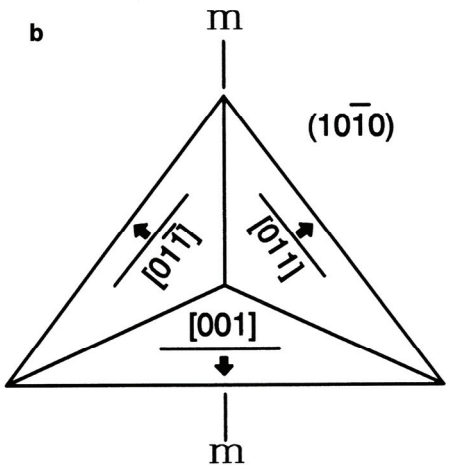

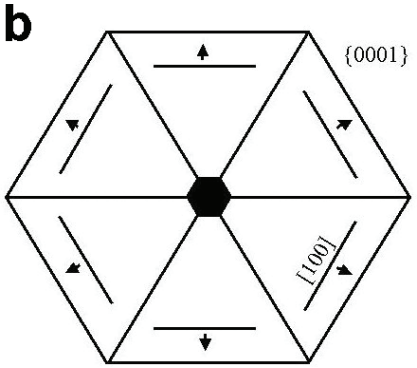

Figure 6 (left). (a) Differential interference contrast (DIC) photomicrograph of a trigonal growth hillock on a {100} face of apatite from the Golconda Mine, Minas Gerais Brazil. The three vicinal faces of the hillock exhibit macrosteps. The horizontal steps run in the [001] direction. The three step orientations are parallel to the three dominant step orientations of the spiral in Figure 5. Image is approximately 666 μm across. (b) Schematic of the face symmetry with respect to the hillock in a. Steps on the basal vicinal face parallel [001]. Lines within each vicinal face represent the orientations of growth steps. Arrows indicate the directions of advancement of steps during growth. [Modified after Rakovan and Reeder (1994)].

Figure 7 (right). (a) DIC photomicrograph of a hexagonal growth hillock on a {001} face of an apatite from the Siglo XX Mine, Llallagua, Bolivia. Steps that form the six vicinal faces run in the <100> directions. Image is approximately 1.2 mm across. (b) Schematic of the face symmetry with respect to the hillock in a. A six-fold axis of rotation perpendicular to {001} symmetrically equates steps of the six vicinal faces. Lines within each vicinal face represent the orientations of growth steps. Arrows indicate the directions of advancement of steps during growth. [Modified after Rakovan and Reeder (1994)].

well-developed hexagonal growth hillocks with six pyramidal vicinal faces (Fig. 7a). The vicinal faces of these hillocks are composed of steps that strike parallel to <100>, all of which are symmetrically related by a six-fold axis of rotation perpendicular to {001} (Fig. 7b). Akizuki et al. (1994) report similar hillocks on the {001} faces of apatites from the Asio Mine, Japan. The {001} faces of hydrothermal apatites commonly exhibit six-sided hillocks such as those in Figure 7. Symmetry and structural nonequivalence of

growth steps on different crystal faces or on a single crystal face have important implications for growth kinetics and trace element incorporation (see sections below on growth rates and surface structural controls on trace element incorporation during growth).

Dissolution. As with crystal growth, dissolution of apatite can lead to surface microtopographic features that are indicative of the dissolution mechanism and also yield information about structural defects in the crystals. In a study of the dissolution of large fluorapatite crystals from Cerro de Mercado, Mexico, in hydrochloric and citric acids, Thirioux et al. (1990) observed the formation of well defined, polygonized etch pits on {100} and {001} surfaces. Regular hexagonal etch pits form on the {001} and uniformly increase in size as dissolution progresses. Etch pits with a trapezohedral geometry form on the {100} surfaces and anisotropically expand along [001] as dissolution continues, resulting in elongate etch troughs. Natural elongate etch pits of a similar morphology were reported on the {100} faces of apatites from Minas Gerais, Brazil (Rakovan and Reeder 1994). The formation of such microtopography suggests the presence and role of dislocations in the dissolution mechanism. Phakey and Leonard (1970) studied the structural defects in Mexican apatites (probably from Cerro de Mercado based on sample description) using X-ray diffraction topography. The dislocation density of the crystals was found to be low, with the majority of dislocations aligned with [001]. Preferential etching of such dislocations explain the morphology of etch pits observed on {001} and {100} surfaces.

APATITE CRYSTAL GROWTH FROM SOLUTION

Geologically, apatite precipitates from melts, concentrated hydrothermal brines, low-temperature aqueous solutions and possibly from the vapor phase (McConnell 1973). Biologically the phase precipitates from intra- and extra-cellular fluids, influenced by a variety of organic molecular species (Skinner 1987, Christoffersen and Landis 1991, McConnell 1973, Elliott 1994). In the laboratory, apatite synthesis is carried out by an array of techniques that includes melt, solution and plasma growth (Gross and Brendt, this volume; Elliott 1994 and references therein). With such a wide variety of environments of formation, it is not unexpected that the kinetics and mechanisms of growth also vary widely. In this section the growth of apatite in aqueous fluids is reviewed. It is in solution growth where the structure and chemistry of the apatite surface is found to exert the greatest influence on the growth process. Most studies of apatite growth from solution have focused on hydroxylapatite. This has been driven by motivation to understand apatite formation in biological systems. Solution growth of geologic apatite is important in surface water, sedimentary and hydrothermal environments. Chlorapatite growth kinetics are rarely addressed.

Precipitation or the formation of apatite begins with nucleation and continues through growth. There is an obvious continuum between nucleation and growth; however, the processes are different in their energetics and mechanisms, which are dependent on many variables, from the type of growth environment to subtle differences within a given environment. Several of the steps involved in precipitation are associated with all mechanisms in all environments. Nucleation must occur and a critical size must be reached by the crystal nucleus so that growth of a stable crystal can continue. Mineral constituents must move from the surrounding environment to the crystal surface. Attachment of these constituents to the surface may be followed by surface diffusion, binding at surface sites of incorporation (protosites) and dissociation of complexing ions from solution. Eventually, burial leads to incorporation and increases in crystal size and volume. [General aspects of nucleation and growth have been reviewed by Nancollas (1979), Nielsen (1984), Nancollas (1984), and Boistelle and Astier (1988).]

NUCLEATION

The driving force for nucleation and crystal growth from solution can be expressed as the positive difference between the chemical potential of a species in a supersaturated solution and that of a saturated solution. Once a solution becomes supersaturated with respect to a particular mineral, 3-D nucleation may occur. For the spontaneous formation of an apatite nucleus (for the sake of discussion we will refer to fluorapatite) in solution the change in the Gibbs free energy (ΔG) of the reaction

$$5\ Ca_{(aq)} + 3\ (PO_4)_{(aq)} + F_{(aq)} \rightarrow Ca_5(PO_4)_3F_{(s)} \quad (1)$$

must be negative. The change in the Gibbs free energy of this crystallization reaction (ΔG_c) can be expressed as

$$-\Delta G_c = R\,T\,\ln S \quad (2)$$

where R is the universal gas constant, T is the absolute temperature, and S is the saturation ratio (Nielsen 1984) defined as

$$[x]S = \left(\frac{[Ca]^5[PO_4]^3[F]}{{}_{eq}[Ca]^5\,{}_{eq}[PO_4]^3\,{}_{eq}[F]} \right)^{\frac{1}{\nu}} = \left(\frac{IAP}{K_s} \right)^{\frac{1}{\nu}} \quad (3)$$

where [x] is the activity of species x in solution, ${}_{eq}[x]$ is the activity of species x in solution at equilibrium, ν = the number of ions in the formula unit of apatite [$\nu = 9$ for fluorapatite as expressed in Equation (1)], IAP is the ion activity product and K_s is the equilibrium constant for Reaction (1), which is equivalent to the solubility product. Saturation, S, can be defined in different ways. Throughout the text S is defined as in Equation (3) unless otherwise noted.

The free energy of the formation of a crystal has two components

$$\Delta G_c = \Delta G_{bulk} + \Delta G_{surf} \quad (4)$$

due to the energy gained by the formation of bonds (ΔG_{bulk}) and the work required to increase surface area (ΔG_{surf}). For a supersaturated solution ΔG_{bulk} is negative and ΔG_{surf} is always positive. The ΔG_{surf} has a geometric component that describes the surface area and that depends on the shape of the nucleus. For a spherical nucleus

$$\Delta G_{surf} = 4\pi r^2\gamma \quad (5)$$

where γ is the interfacial or surface free energy, which is assumed to be independent of nucleus/crystal size. During nucleation the surface free energy makes up a large part of the total free energy of the nucleus (Boistelle and Astier 1988). This positive surface contribution to the free energy acts as an energy barrier to nucleation, and is why supersaturation is necessary for a nucleus to form (Fig. 8). The interfacial energy, γ, of apatites has been studied by a variety of different methods including crystal growth and dissolution as well as surface wetting experiments. The obtained values vary widely depending on the method of determination.

Surface free energies of hydroxylapatite and fluorapatite were determined by Busscher et al. (1987) from contact angle measurements. They found that in vacuum γ ranges between 72 and 95 mJ/m^2. In the presence of a saturated vapor, γ was found to be between 28 and 48 mJ/m^2. The difference in γ obtained by the two methods was explained as resulting from the presence of an adsorbed film originating from the liquid droplets employed in the measuring procedure. Face-specific measurements revealed for the {001} crystal face $\gamma = 28 \pm 3$ mJ/m^2, and $\gamma = 48 \pm 7$ mJ/m^2 on {100} for fluorapatite, and for hydroxylapatite the {001} crystal face $\gamma = 39 \pm 11$ mJ/m^2, and $\gamma = 30 \pm 3$ mJ/m^2 on

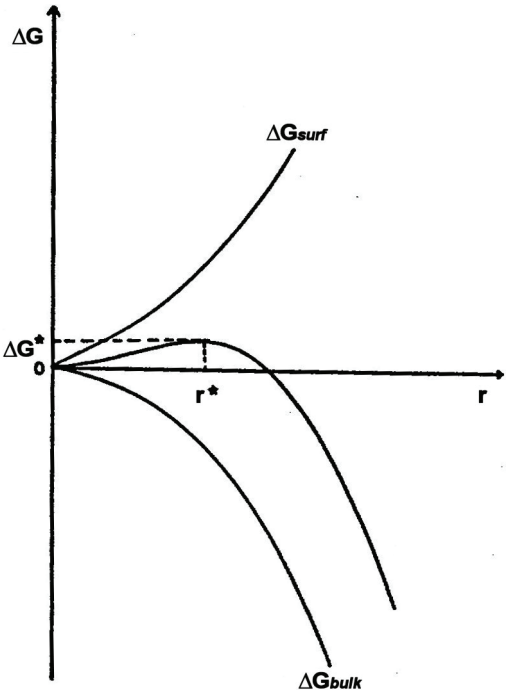

Figure 8. A plot of the change in Gibbs free energy, ΔG, with size of a crystal, r. The activation energy ΔG* must be reached for the creation of a nucleus of critical radius r*.

{100}. For hydroxylapatite, Arends et al. (1987) calculated from growth rate data $\gamma = 87$ mJ/m^2 and 80 mJ/m^2 at pH = 7 and 6, respectively. On a theoretical basis, Christoffersen et al. (1991) calculated the surface free energy of fluorapatite to be 250 mJ/m^2. This is most closely approximated by the results of Vancappellen and Berner (1991), who conducted seeded fluorapatite growth rate experiments in a carbonate-free simulated seawater solution. From analysis of their kinetic data they calculated the $\gamma = 289$ mJ/m^2. Christoffersen and Christoffersen (1992a) developed a revised version of the rate model of Hilig (1966) for the growth of crystals by a nucleation and spread mechanism, which included the relationship of surface free energy and solubility. The model was applied to the rate of growth of hydroxylapatite, and γ was calculated to be 80 mJ/m^2. Christoffersen and Christoffersen (1992b) found the same for supersaturations between 3.25 and 7.53. They suggested that the deviation of this value from the value expected from theory, 250 mJ/m^2, is the result of imperfections in the crystal surfaces. Liu and Nancollas (1996) calculated an interfacial free energy $\gamma = 30$ mJ/m^2 from their growth kinetic data, and they determined $\gamma = 18.5$ mJ/m^2 from contact angle measurements. The surface free energy of fluorapatite was found to be 120 mJ/m^2 from the growth results and 42 mJ/m^2 from the dissolution results in kinetic experiments by Christoffersen et al. (1996a). For hydroxylapatite, Christoffersen et al. (1998b) determined $\gamma = 100$ mJ/m^2 (from growth kinetic data) and $\gamma = 40$ mJ/m^2 (from dissolution kinetic data). This difference in γ values has been explained by Christoffersen et al. (1998b) and Christoffersen and Christoffersen (1992a) by the presence of surface imperfections that they conclude will affect the rate of dissolution to a greater extent than the rate of growth.

Interfacial free energy is of critical importance in determining the thermodynamics and kinetics of nucleation and crystal growth (Stumm and Morgan 1996). It is particularly important in understanding controls on crystal morphology, rate-limiting steps in the growth process, and the interactions with adsorbed species from solution. It is obvious from the review above, that there is considerable uncertainty in the value of the surface free energy of apatite. Although values vary widely, those determined from growth data are generally higher than those determined from dissolution kinetics, and γ values for fluorapatite are higher than for hydroxylapatite.

In homogeneous nucleation a crystal nucleus forms free from contact with another solid. One mechanism by which the energy barrier to nucleation, ΔG^* in Figure 8, can be decreased is by heterogeneous nucleation, where the surface of another material (i.e., another crystal) acts as a substrate on which nucleation occurs. The interaction of the substrate surface with adsorbates decreases the surface free energy of a nucleus (Boistelle and Astier 1988). For polynuclear growth (see growth mechanisms below) of hydroxylapatite Christoffersen and Christoffersen (1992a) calculated the critical radius of the surface nuclei as $2.8 < r^* < 5.1$ Å from growth kinetic data. In the simplest case of heterogeneous nucleation, the influence of the substrate is only on the energy of nucleation and no specific orientational relationship occurs between the substrate and the overgrowth. However, in many cases the structure of a crystalline substrate may also have an influence on the orientation of the nucleus and crystal overgrowth. When the substrate dictates the orientation of an overgrowth, it is known as epitaxy. Epitaxy occurs when one or more of the structural dimensions on the surface of the substrate matches, or is very close to, one or more of the structural dimensions in the overgrowth. In such a case the lowest energy configuration is often one in which the directions of similar structural dimension in the two phases are in register. Hence, there is a control on the orientation of the overgrowth as it forms. Homoepitaxy, the growth of a mineral on a preexisting substrate of the same mineral, is essentially crystal growth by a layer mechanism and is the basis for the use of seeds in growth experiments.

GROWTH MECHANISMS

Once a stable nucleus has formed, a crystal can continue to grow by several different mechanisms. All mechanisms of crystal growth involve diffusion of adatoms or growth units from the bulk of the growth medium through a diffusion boundary layer to the crystal surface and adsorption thereon. In the case of growth from solutions of extremely high supersaturation, the crystal surface can be atomically rough. In this situation, adsorption and incorporation of growth units may occur with equal probability at all exposed attachment sites with little or no surface diffusion after attachment. Such attachment and incorporation leads to macroscopically rough or anhedral crystals, and is called continuous growth. Most apatites, however, do not grow in a regime of such high supersaturation. In the majority of cases, growth occurs by a layer mechanism, where addition of growth units results in the development of planer crystal faces.

One mechanism of layer growth is two-dimensional nucleation (Fig. 9a). Analogous to heterogeneous nucleation, growth units must organize on the crystal face to reach the critical diameter of a surface nucleus, with an associated activation energy barrier. Once this has occurred, the addition of growth units is energetically favored at the edge (step) of this layer nucleus. Kinks in the layer edge are even more favorable for attachment and incorporation. By addition of growth units to edge and kink sites, the new layer spreads over the preexisting face (Fig. 9b). Normal growth of the crystal face proceeds by repeated two-dimensional nucleation and spread. Because of the activation barrier to nucleation, the rate-limiting step in this type of growth is often considered to be the initial two-dimensional nucleation of each progressive layer. Two-dimensional nucleation and growth, also called surface nucleation, birth-and-spread, and nucleated layer growth, can be divided into two categories that will manifest themselves in different reaction rates and rate orders. In the mononuclear case each surface nucleus will spread over the entire crystal face on which it is formed. The polynuclear mechanism involves the formation of multiple surface nuclei. These will interfere with one another before any one can cover the entire surface.

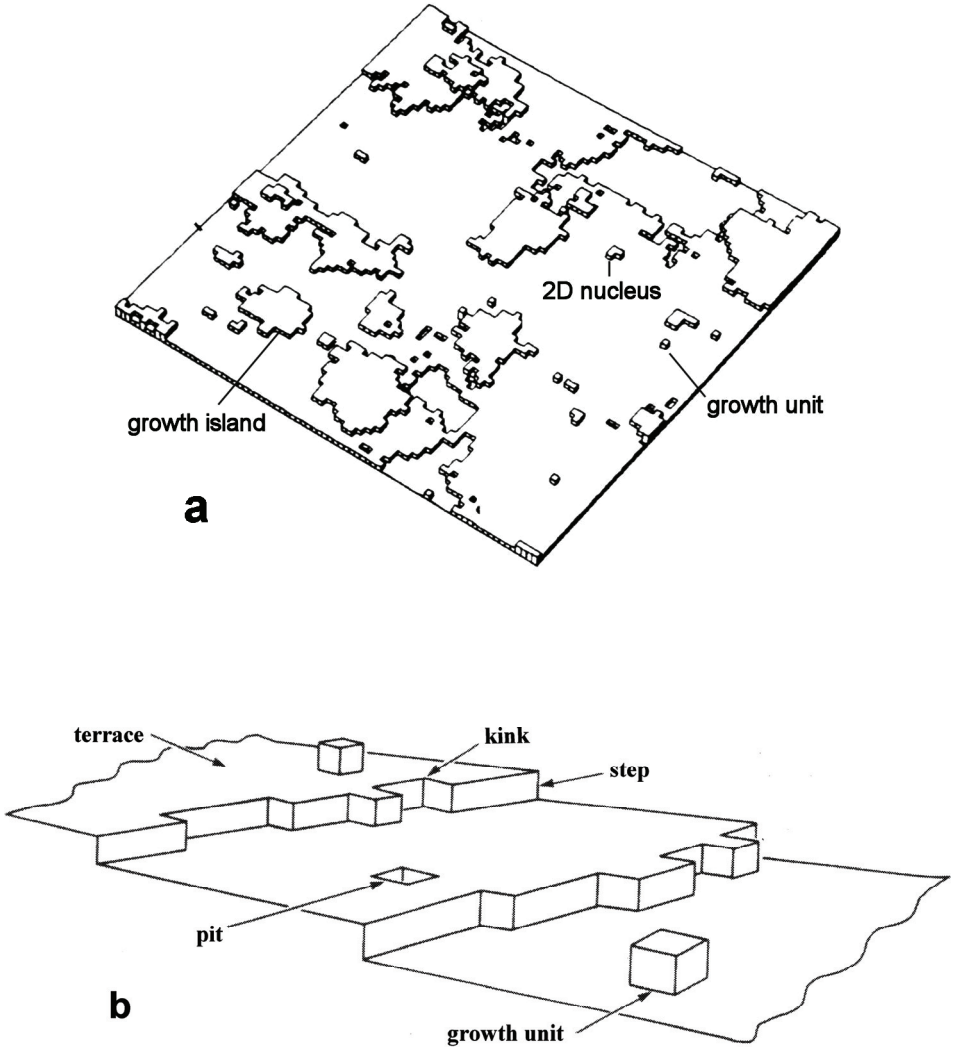

Figure 9. (a) Schematic results of a computer simulation of a crystal surface growing by the birth and spread mechanism. Numerous growth islands form the surface microtopography. [Modified from Gilmer and Jackson (1977).] (b) Schematic of the microtopography on a growing crystal face and the different types of surface sites.

A second type of layer growth is the spiral growth mechanism (Burton et al. 1951). The potential for spiral growth occurs when a screw dislocation or other extended defect in the crystal intersects a crystal face. The displacement of the structure around the dislocation creates a step on the face where the dislocation emerges. Again, for energetic reasons (Burton et al. 1951, Sunagawa 1984), incorporation of adatoms or growth units on the crystal face during growth takes place preferentially along the step, and more specifically at kink sites within the step (Fig. 9b). Because kink sites are the most likely surface sites for eventual incorporation they have been distinguished as proto-bulk sites or simply "protosites" (Nakamura 1973, Dowty 1976). A protosite is the surface representation of a bulk crystallographic site for which the occupant of the site is not yet emplaced or is not fully coordinated. As growth units are added at the step, the step spreads laterally. Because the step terminates at the dislocation, the step will spiral during growth, hence the name spiral growth. One common manifestation of spiral growth is the formation of a surface microtopographic spiral (Figs. 10 and 5). The presence of a growth spiral on a crystal face is thus an indication that the face has grown by the spiral mechanism.

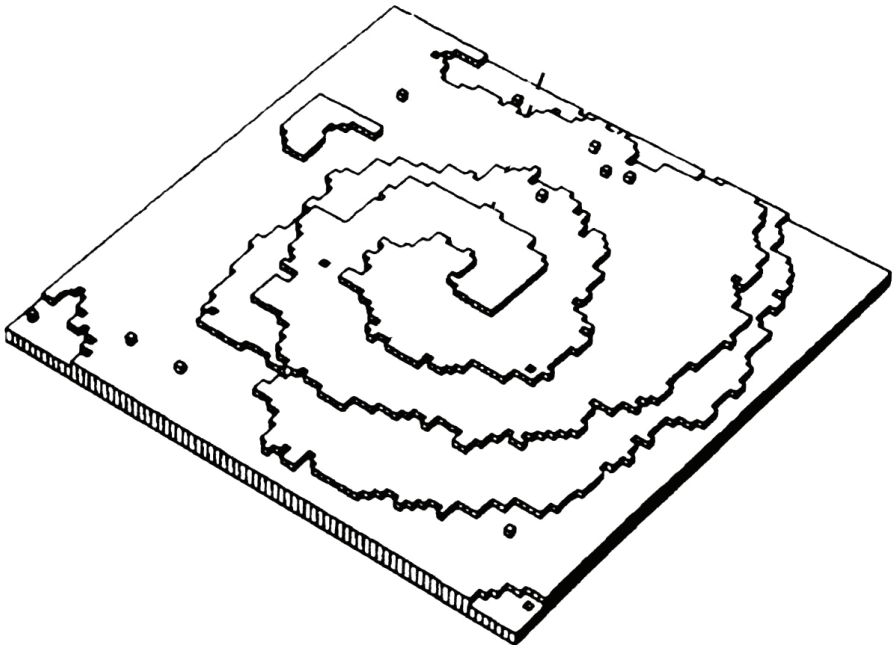

Figure 10. Results of a computer simulation of a crystal surface growing by the spiral growth mechanism. A growth spiral forms the surface microtopography. [Used by permission of Elsevier Science Ltd., from Gilmer (1976) *Journal of Crystal Growth*, Vol. 35, Fig. 4d, p. 21.]

In part, the type of growth mechanism that can operate on a given crystal face is dictated by the structure of that face. Periodic bond chain (PBC) theory predicts the possible growth mechanisms of a given face by analysis of the atomic structure of a surface slice parallel to that face (Hartman and Perdok 1955a, Hartman and Perdok 1955b). A PBC is a structural sequence or chain of uninterrupted strong bonds within a structure. Morphologic features such as crystal faces and microtopographic steps on faces are often dictated by the presence and direction of PBCs. A crystal face can be categorized by the number of non-parallel PBCs within a slice parallel to that face. F faces contain two or more PBCs, S faces contain only one PBC, and K faces have no PBCs. In Hartman and Perdok's PBC theory, only F faces should grow by a spiral mechanism. The growth rate of F faces is predicted to be slower than that of S and K faces, hence F faces should dominate the crystal habit.

In an analysis of the apatite structure Terpstra et al. (1986) identified nine different PBCs: <001>, <100>, <101>, <1$\bar{1}$0>, <120>, <121>, <122>, <$\bar{1}$20>, and <$\bar{2}$10>. Twelve different forms, including the {100} and {001}, were identified as F type (Terpstra et al. 1986), and thus by PBC theory can grow by a spiral mechanism (Hartman and Perdok 1955a). In a {100} slice (a monolayer of thickness d_{hkl} deposited on a given face during layer growth) there are PBCs that parallel the directions of the growth spiral steps reported by Amelinckx (1952b) (Fig. 5) and the vicinal face steps on growth hillocks reported by Rakovan and Reeder (1994) (Fig. 6). Growth step directions of hexagonal hillocks on the {001} face of apatite (Rakovan and Reeder 1994, Akizuki et al. 1994) (Fig. 7) were also identified as PBCs in the {001} slice.

The growth mechanism of a crystal will vary depending on factors that include the surface and step free energies of the crystal faces, the nature and density of defects within the crystal, and most importantly the degree of supersaturation, S, of solution. Figure 11 shows the relationship between S and growth mechanism. In this figure theoretical

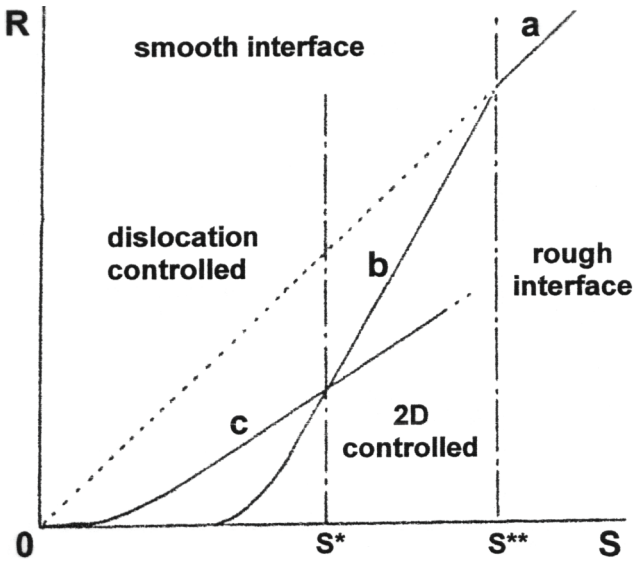

Figure 11. Illustration of the relationship between growth rate, R, and super-saturation, S. Curve a for continuous growth; curve b for a birth and spread growth mechanism; and curve c for a spiral growth mechanism. The vertical lines at S* and S** indicate the transitions from growth dominated by the spiral mechanism and the birth-and-spread mechanism, respectively. [Modified after Sunagawa (1984).]

growth rate curves are plotted for spiral growth (c), 2-D nucleation and spread (b) and continuous growth (a). The values of S* and S** are system dependant and represent the saturation states where the dominant growth mechanism changes from spiral growth to 2-D nucleation and spread, and from 2-D nucleation and spread to continuous growth, respectively. The mechanism by which apatite grows has been extensively studied (discussed later). Most of this work is based on inferences made from the reaction orders from growth kinetic data. Several studies, however, have used direct observation of growth *in situ* or the surface microtopography to determine the mechanism of growth on specific crystal faces.

Solubility, equilibrium, and precursor phases in apatite growth

The hydroxylapatite-solution reactions of growth and dissolution depend on the solubility of apatite and other phases in the $Ca(OH)_2$-H_3PO_4-H_2O system. In this system, hydroxylapatite is the thermodynamically most stable calcium orthophosphate phase at normal Earth-surface conditions and in most biological systems. Figure 12 (from Elliott 1994) shows an example of calculated solubility isotherms of the orthophosphates at 37°C. The exact positions of the isotherms depend on the ionic strength of the solutions and the thermodynamic constants used to calculate them (solubility products and stability constants). Solubility data for apatites vary widely and identification of ideal solubility constants has been difficult. This is particularly true of hydroxylapatites. Table 1 gives a sampling of published solubility products, K_s, for fluorapatite and hydroxylapatite. Chander and Fuerstenau (1984) review solubility measurements of hydroxylapatite made through 1978 and suggest that there is good agreement that the solubility product of stoichiometrically pure, well-crystallized hydroxylapatite is $1 \times 10^{-57.5}$. Apatite can incorporate large amounts of impurities and structural defects that lead to varying degrees of non-stoichiometry, which in part has lead to varying solubility measurements. At low pH values dicalcium phosphates become more stable than hydroxylapatite (Fig. 12). Nancollas (1984) suggests that in hydroxylapatite dissolution experiments conducted at low pHs, apatite may form a surface coating of a more acid phosphate. Determination of solubility will then reflect the surface phase and not apatite. Reaction kinetics can be slow for the calcium orthophosphates and make determination of equilibrium difficult. It has also been shown that kinetic factors may play a more important role in growth and dissolution reactions than has been traditionally accounted for. All of these factors may in part account for the discrepant solubility data for apatites in the literature (Table 1).

Table 1. A sampling of published solubility products, K_s, for fluorapatite, FAP [$Ca_5(PO_4)_3F$] and hydroxylapatite, HAP [$Ca_5(PO_4)_3OH$].

Reference	*Phase*	K_s	*Temp. (°C)*
Jaynes et al. (1999)	HAP	$1 \times 10^{-56.02}$	20-25
Valsami-Jones et al. (1998)	HAP	1×10^{-58}	25
Elliott (1994): *calculated*	HAP	2.57×10^{-63}	25
Chander & Fuerstenau (1984)	HAP	$1 \times 10^{-57.5}$	25
Nancollas (1982)	HAP	4.7×10^{-59}	25
Stumm & Morgan (1981)	HAP	$1 \times 10^{-57.0}$	25
Snoeyink & Jenkins (1980)	HAP	$1 \times 10^{-55.9}$	25
*Fawzi et al. (1978)	HAP	1×10^{-61}	30
*McDowell et al. (1977)	HAP	$1 \times 10^{-88.5}$	25
*Brown et al. (1977)	HAP	1×10^{-57}	?
*Wu et al. (1976)	HAP	$1 \times 10^{-62.5}$	30
*Smith et al. (1976)	HAP	$1 \times 10^{-58.5}$	20
*Avnimelech et al. (1973)	HAP	$1 \times 10^{-58.2}$	25
*Saleeb & deBruyn (1972)	HAP	$1 \times 10^{-57.5}$	?
*Chien (1972)	HAP	$1 \times 10^{-60.5}$	25
*Weir (1971)	HAP	$1 \times 10^{-58.5}$	25
Jaynes et al. (1999)	FAP	$1 \times 10^{-58.13}$	20-25
Valsami-Jones et al. (1998)	FAP	$\sim 1 \times 10^{-70}$	25
Elliott (1994): *calculated*	FAP	$2.50 \times 10^{-68.5}$	25
Chin & Nancollas (1991)	FAP	9×10^{-61}	37
Driessens (1982)	FAP	$1 \times 10^{-60.6}$	25
Amjad et al. (1981)	FAP	$1 \times 10^{-60.15}$	37
Stumm & Morgan (1996)	FAP	$1 \times 10^{-59.0}$	25
Lindsay (1979)	FAP	$1 \times 10^{-58.89}$	

* Taken from tabulated values in Chander & Fuerstenau (1984).

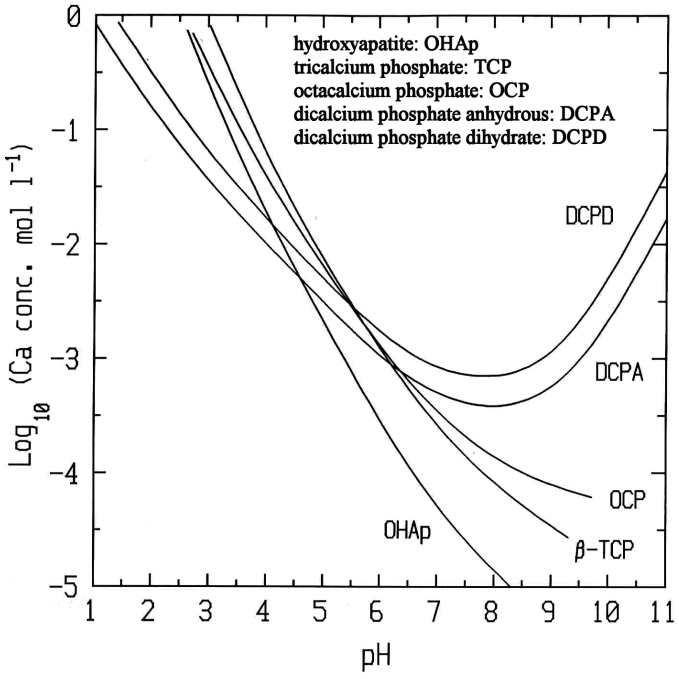

Figure 12. Solubility iso-therms of calcium ortho-phosphate phases in the sys-tem $Ca(OH)_2$-H_3PO_4-H_2O at 37°C (equimolar calcium and phosphate). [Modified after Elliott (1994).]

Many calcium phosphate solutions prepared for hydroxylapatite growth experiments and possibly some natural solutions are supersaturated with respect to other calcium orthophosphates such as tricalcium phosphate, TCP [$Ca_3(PO_4)_2$], octacalcium phosphate, OCP [$Ca_4H(PO_4)_3$], dicalcium phosphate anhydrous, DCPA ($CaHPO_4$), and dicalcium phosphate dihydrate, DCPD ($CaHPO_4 \cdot 2H_2O$). Slightly acidic to basic solutions that are supersaturated with TCP, OCP, or DCP will also be supersaturated, to a higher degree, with hydroxylapatite (Fig. 12). The activation barrier to nucleation of a phase is directly related to the free energy of a surface, or more appropriately described as the surface-solution interfacial free energy. The activation barrier to nucleation, and hence the degree of supersaturation necessary to overcome this barrier and form a nucleus, generally increases with increasing surface free energy. Thus it is possible for a thermodynamically less stable phase to nucleate and grow if its surface free energy is significantly less than that of a more stable phase. This is often times seen in the precipitation of calcium phosphates. In many cases hydroxylapatite formation is preceded by the precipitation of another, less stable calcium phosphate, which may ultimately transform to apatite. Numerous studies have noted that a precursor phase to the formation of hydroxylapatite can be an amorphous calcium phosphate phase, ACP (Eanes et al. 1966, Brecevic and Furedi-Milhofer 1972, Termine et al. 1970). Francis and Web (1971) proposed DCPD as a precursor. Eanes et al. (1966) suggested TCP as a precursor and Brown (1966) suggested OCP. Many studies have proposed various mixtures of hydroxylapatite and other precursor phases, especially OCP, to explain the nonstoichiometry of some synthetic and natural bio-hydroxylapatites (Brown 1966, Young and Brown 1982 and references therein). The ribbon-like habit of biological apatites (Fig. 3) has also been used to indicate that OCP was a precursor (Brown 1966). More recent studies that involve hydroxylapatite precipitation experiments have shown that different precursor phases can form depending on solution conditions, particularly depending on saturation state with respect to hydroxylapatite and other calcium orthophosphates.

Boskey and Posner (1973) synthesized ACP and studied the kinetics of its transformation to hydroxylapatite as a function of pH at 26°C and as a function of temperature at a pH of 8. The rate of transformation increases with increasing pH. The mechanism of transformation is dissolution of the ACP and reprecipitation of hydroxylapatite, with the energetically least favorable and rate-limiting step in the process being the nucleation of hydroxylapatite. The activation energy of this conversion was determined as 33 kcal/mol, which includes nucleation and the energy associated with the dissolution of ACP. In seeding experiments there was no measurable induction period, in contrast to the unseeded experiments. This indicates that the activation barrier to ACP dissolution is relatively small and that the 33 kcal/mol is dominated by the barrier to hydroxylapatite nucleation. The rate of conversion increases proportionally with the amount of hydroxylapatite already formed (hence the apatite surface area), suggesting that the process of conversion was autocatalytic. Boskey and Posner (1976) homogenously precipitated hydroxylapatite in solutions with supersaturations (defined in this study as $S = [IAP - K_{sp}/K_{sp}]$, see discussion of growth rates) from 22 to 47, pH = 7.4, temperature = 26.5°C, and ionic strengths 5.0-0.005 M. Hydroxylapatite was found to precipitate without the formation of ACP as a precursor. This is in contrast to high supersaturations ($S = [IAP - K_{sp}/K_{sp}] = 500$) and pH = 6.8 where ACP did form first (Boskey and Posner 1973). Nancollas and Tomazic (1974), working in the same range of solution conditions as Boskey and Posner (1976), found direct hydroxylapatite precipitation in experiments with large seeds, and they found OCP directly precipitated on the seed crystals at higher supersaturations than in Boskey and Posner (1976). They conclude from their work and the work of others that pH, Ca and PO_4 concentrations and ratios, ionic strength, temperature and the presence of seeds are all critical in determining

the initial precipitate.

Feenstra and Bruyn (1979) studied the dependence of the induction period between ACP and hydroxylapatite on the degree of S and pH, in high supersaturations, where precursor phases form before hydroxylapatite (26°C, ionic strength of 0.15 mol/L, and pHs 6.7, 7.4, and 8.5). They found the first step was nucleation of ACP followed by OCP as an intermediate phase in the conversion of ACP to hydroxylapatite. They pose the possibility that ACP acts as a substrate for the heterogeneous nucleation of OCP and the OCP acts as a substrate for the heterogeneous nucleation and epitaxial overgrowth of hydroxylapatite. Koutsoukos et al. (1980) studied the crystallization of hydroxylapatite using a constant composition method. In experiments with differing amounts of seed crystals, varying Ca/P ratios, pH from 6-8.5, 37°C, and constant ionic strength in solutions supersaturated with hydroxylapatite only, they found that hydroxylapatite was precipitated on the seed crystals without the formation of a precursor phase. In similar solutions that were also supersaturated with TCP, TCP was never convincingly identified. Amjad et al. (1981) conducted experiments similar to those of Koutsoukos et al. (1980) for fluorapatite and found that no precursor phases were observed in this range of super-saturations.

Christoffersen et al. (1989) investigated the formation of calcium-deficient hydroxylapatite. In their precipitation experiments they found that ACP and in some cases DCPD (at low temperature, 15°C) were the initial precipitates. The original ACP (ACP1) transformed to a second ACP form (ACP2), which in turn transformed to OCP and finally to hydroxylapatite. These transformations are thought to be solution-mediated where one phase dissolved as the following phase precipitated. Transformation rates increased with temperature. Lundager-Madsen and Christensson (1991) studied calcium phosphate precipitation in the pH range of 5-7.5 at 40°C with Ca and PO_4 concentrations up to 0.04M. ACP was the first solid phase to precipitate in most of their experiments. At low pH brushite ($CaHPO_4 \cdot 2H_2O$) is the only precipitate, and at low concentrations OCP dominates. ACP ultimately transforms to brushite or hydroxylapatite.

It is evident from growth experiments and observations of natural calcium phosphates that precursor phases such as ACP, TCP, OCP, or DCP can be involved in the precipitation of hydroxylapatites at low temperature conditions. The presence of these phases, mixed with apatite, has, in part lead to the difficulty in making accurate solubility measurements of apatites.

The formation of precursor phases is in accordance with Oswald's rule of stages for multiple phase precipitation of sparingly soluble salts. In a system like the orthocalcium phosphates, the phase with the highest solubility and lowest surface free energy, which means that it will be at the lowest supersaturation at a given set of conditions, is preferentially formed due to more favorable kinetics. Ultimately, thermodynamic factors will drive the system to formation of a more stable phase. Thus, ACP, OCP, etc. may initially form in supersaturated solutions but these phases will ultimately transform to apatite.

Growth rates

The growth rate for many sparingly soluble salts, $M_{\nu+}A_{\nu-}$, can be expressed as:

$$\frac{d(M_{\nu+}A_{\nu-})}{dt} = -ks[([M]^{\nu+}[A]^{\nu-})^{1/\nu}] - [([M]_{eq}^{\nu+}[A]_{eq}^{\nu-})^{1/\nu}]^n \quad (6)$$

where [x] is activity and $[x]_{eq}$ is the activity at equilibrium, k is the precipitation rate constant, s is proportional to the number of available growth sites on a seed or crystal (reactive surface area), $\nu = (\nu+ + \nu-)$, and n is the reaction order (Inskeep and Silvertooth

1988). Thus for fluorapatite

$$5\ Ca_{(aq)} + 3\ (PO_4)_{(aq)} + F_{(aq)} \rightarrow Ca_5(PO_4)_3F_{(s)} \quad (1)$$

$$\frac{d(Ca_5(PO_4)_3F)}{dt} = -ks[([Ca]^5[PO_4]^3[F])^{1/9}] - [([Ca]_{eq}^5[PO_4]_{eq}^3[F]_{eq})^{1/9}]^n \quad (7)$$

From growth kinetic theory, distinction between different growth mechanisms and the rate-limiting step during growth is often inferred on the basis of reaction order. If the rate-limiting step in the growth process is diffusion of growth units through the solution, $n = 1$. Rates controlled by spiral growth will have $1 < n \leq 2$, and for surface nucleation and spread mechanisms n is assumed to be greater than 3.

Determination of growth mechanism from rate data. Most determinations of the growth mechanisms of apatites precipitated in solution experiments are based on fitting kinetic data (usually changes in solution chemistry with time) to empirical rate equations in pure systems. From crystal growth theory the order of these rate equations depend on the growth mechanism and hence can be used to infer the dominant mechanism active in the experiment. Most apatite growth rate experiments have involved precipitation of hydroxylapatite. Nancollas (1979) used the semi-empirical equation $R = d[Mv + Av-]/dt = -ks[(IAP)^{1/v} - Ksp^{1/v}]^n$ and found for hydroxylapatite grown by the constant composition method at pH 5.0-6.5 and supersaturations, S, between 2 and 7, that the overall growth rate was proportional to (S-1). From this relationship they suggested that growth occurred by the spiral mechanism. Koutsoukos et al. (1980) fit their rate data with the same rate equation and determined the reaction order n = 1.25 for low hydroxylapatite super-saturations; again, indicating growth by the spiral mechanism. They also found that chemistry of the precipitate was independent of the Ca/P ratio of the solution. Moreno (1981) studied the dependence of the kinetics of hydroxylapatite growth on the concentration of seed crystals and the degree of supersaturation, S. Seeded growth experiments were conducted in solutions at 37°C, pH = 7.4, S_{HA} = 15.9, 11.9 and 5.32, and Ca:PO_4 of 5:3 and 3:5 at varying seed concentrations. They found that the rates of precipitation were highly dependent on the amount of seeds added, hence total surface area. The ratio of Ca:PO_4 at the same S_{HA} did not affect the rate of hydroxylapatite formation but may have influenced the precursor formation of OCP. Diffusion-limiting and 2-D nucleation models did not fit their data, although a spiral growth model did. Inskeep and Silvertooth (1988) studied seeded hydroxylapatite precipitation at S = 7.7-21.4, pH 7.4-8.4 (geochemically relevant in earth surface conditions), and using the model of Nielsen and Toft (1984) they predicted growth by the spiral mechanism. A rate equation was developed on the basis of the reaction orders determined with respect to solution species: $R = k_f s\gamma_2\gamma_3[Ca^{2+}][PO_4^{3-}]$, where k_f = rate constant for the forward reaction, s = surface area, and γ_2 and γ_3 are the divalent and trivalent species, Ca^{2+} and PO_4^{3-}, with ion activity coefficients calculated from the Davies equation (Davies 1962). This equation is first order in $[Ca^{2+}]$, $[PO_4^{3-}]$ and s. The average rate constant k_f was determined to be 173 ± 11 $L^2\ mol^{-1}\ m^{-2}\ sec^{-1}$. The apparent Arrhenius activation energy was determined over a temperature range of 10 to 40°C to be 186 ± 15 kJ mol^{-1}. Inskeep and Silvertooth (1988) speculated that the rate-limiting step is a surface process, specifically that it is the surface diffusion of Ca and PO_4 ions and dehydration commensurate with binding at surface sites of incorporation. Using a constant-composition method and seeded solutions with S_{HA} = 3.05-5.58 Koutsopoulos (2001) found hydroxylapatite formed without a precursor phase. The spiral growth model was found to best fit their kinetic data.

In contrast to the above studies where the growth mechanism was inferred to be spiral growth, Arends et al. (1987), using the constant composition technique of Hohl et

al. (1982) studied the rate of crystal growth of hydroxylapatite at 37 °C, pHs of 6.0 and 7.0 and supersaturations S = 2 - 6. Reaction orders n = 3.2 and 2.9 for experiments at pH = 7 and 6 respectively were determined. It was concluded that hydroxylapatite grew by the polynuclear mechanism in these experiments. The rate of growth differed by a factor of two between these two pH values. Christoffersen and Christoffersen (1992a) developed a revised version of the model of (Hilig 1966) for the growth of crystals by a nucleation and spread mechanism. In their model growth rates are expressed in activities of solutes rather than concentrations, and the relationship of surface free energy and solubility is built into the rate expression. The model was then applied to the rate of growth of hydroxylapatite (Christoffersen and Christoffersen 1992b). Rate data from their experiments at supersaturations between 3.25 and 7.53 are consistent with growth controlled by a surface process. Two models, the spiral growth model and the polynuclear model, were found to be consistent with the results. Using their revised growth model, the frequency of ion integration was found to be 9×10^4 s^{-1} for the polynuclear model, close to the 1.6×10^5 s^{-1} value expected if the rate-determining step is partial dehydration of calcium ions. If similar assumptions to those used for the application of the polynuclear theory are applied to the spiral theory, similar values of the ion integration frequency are obtained, making it difficult to distinguish the rate-controlling mechanism. Christoffersen et al. (1998a) used the revised mechanistic model of polynuclear growth, developed by Christoffersen et al. (1996b), to fit the growth of hydroxylapatite. In this study they make the assumption that the incorporation of OH ions strongly influences the growth of hydroxylapatite. They propose that H_2O is initially incorporated into the column anion position and that OH formation takes place by deprotonation after burial. It is suggested that this will then slow the further incorporation of Ca ions at kink sites on the surface. Christoffersen et al. (1998b) examined the role of varying Ca:PO_4 ratios (from 0.1-20) in solution on the kinetics of hydroxylapatite growth at pHs of 6 and 7.2, and supersaturations S = 3.03-6.86. Again, they modeled their kinetic results with a polynuclear growth mechanism in which nucleation is expressed as a function of mean-ion activity and OH formation by H_2O dissociation in the growth layer is taken into account.

Although the number of studies of fluorapatite growth kinetics is smaller than for hydroxylapatite, they have particular relevance to sedimentary apatite formation. Amjad et al. (1981) repeated the experiments of Koutsoukos et al. (1980) (pH = 7.40, T = 37°C, S = 10-30) for fluorapatite and similarly found that the rate equation held for FAP with an apparent reaction order of 1.25 indicating a spiral growth mechanism. Van Cappellen and Berner (1991) conducted seeded fluorapatite growth rate experiments in a carbonate-free simulated seawater solution at different degrees of saturation, S. They fit their growth rate data with an empirical rate law of the form

$$r = K_a(S - 1)^n \tag{8}$$

where r is the growth rate (in units of mass of fluorapatite per unit time and unit seed surface area), and K_a is an apparent rate constant. It was found that for supersaturations S <37 the reaction order n = 1.8 ± 0.3, and for S > 37 n = 4.9 ± 0.4 (Fig. 13). The slope of the line fit to plots of log (J/m_O) vs. log (1-S) is equal to the reaction order, n, for growth rates that are normalized to surface area. They interpreted this to indicate a transition from growth by the spiral growth mechanism to growth dominated by a polynuclear or two-dimensional nucleation and spread mechanism; thus the saturation value of 37 = S*, where the dominant growth mechanism changes from spiral to two-dimensional nucleation and spread (Fig. 11). Christoffersen et al. (1996a) conducted seeded growth and dissolution experiments with fluorapatite microcrystals in solutions with Ca:P:F = 10:6:2, and 5.0 < pH < 6.5. In contrast to Van Cappellen and Berner (1991) they found

that both growth and dissolution appear to be controlled by a polynuclear surface mechanism in the supersaturation range studied: $2 < S < 7$ for growth and $0.1 < S < 0.7$ for dissolution. They note that the highest supersaturation in Amjad et al. (1981) was in the lower range of those used in Van Cappellen and Berner (1991), yet the rate of growth determined in Van Cappellen and Berner (1991) was approximately 300 times slower than that measured in Amjad et al. (1981). Figure 14 is a plot of the kinetic data from Amjad et al. (1981), Van Cappellen and Berner (1991) and Christoffersen et al. (1996a). The results of Amjad et al. (1981) fit well with those of Christoffersen et al. (1996a).

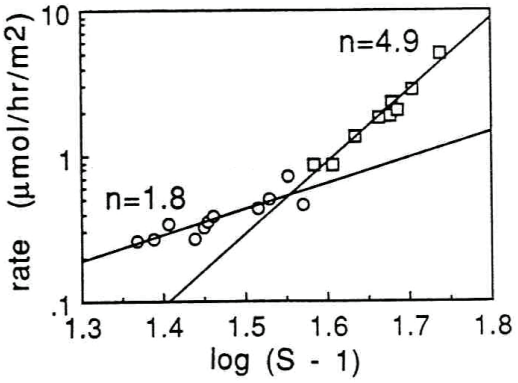

Figure 13. Relationship between growth rate and supersaturation for fluorapatite plotted on a log-log scale. The change in the empirical order of the growth rate, n , indicates a change in the dominant growth mechanism from spiral to birth-and-spread. [Modified after Van Cappellen and Berner (1991).]

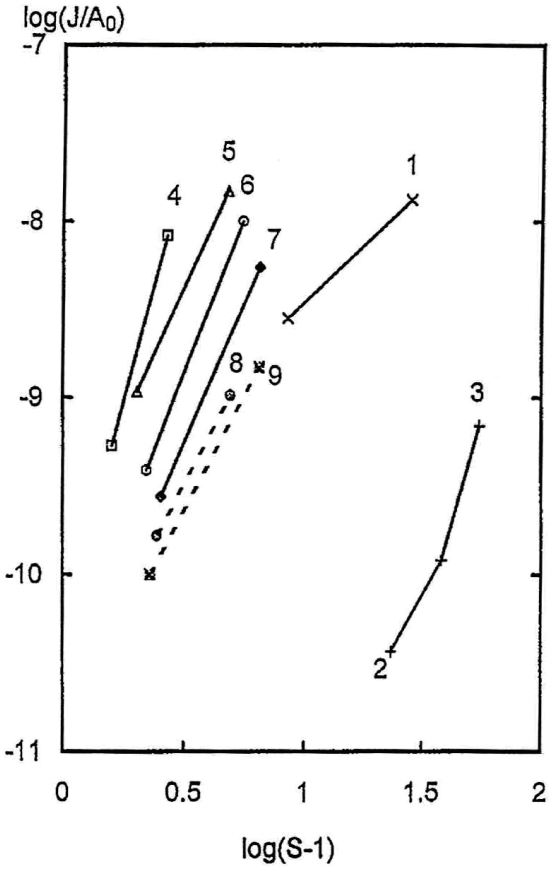

Figure 14. Relationship between growth rate and supersaturation, plotted as the log of the quotient of the overall growth rate, J, and the initial surface area of the seed crystals, A_O vs. the log of the super-saturation S – 1, for apatite from different studies:

Line No. *(Reference)*

1 (Amajad et al. 1981);
2-3 (Van Cappellen & Berner 1991);
4-7 (Christoffersen et al. 1996);
8-9 (Christoffersen & Christoffersen 1992b).

Lines 1-7 are for fluorapatite and 8-9 for hydroxylapatite. [Used by permission of Elsevier Science Ltd., from Christoffersen et al. (1996) *Journal of Crystal Growth*, Vol. 163, Fig. 5, p. 301.]

The influence of impurities on growth kinetics. The presence of impurities in solution, including foreign ions, small molecules and polymers, can have a marked effect on the kinetics of apatite crystal growth (Wu and Nancollas 1998). Chin and Nancollas (1991) investigated the effect of Zn and Mg on the dissolution kinetics of fluorapatite. Dissolution was retarded in the presence of both Zn and Mg ions at pH 5.0; however, Zn was much more effective in inhibiting the dissolution. The effective adsorption affinity, calculated from the decrease in rates of dissolution, was 2.5×10^5 L/mol. Vancappellen and Berner (1991) investigated the affect of Mg^{2+} on fluorapatite growth over the dissolved composition range of 0-60 mM. They found that Mg^{2+} inhibited growth, and in the Mg^{2+} concentration range typically found in marine pore waters (40-60 nM) the rate of growth was slowed by a factor of 15 to 20 compared to solutions free of Mg^{2+}. The inhibition of fluorapatite growth was explained by blocking of active growth sites by adsorbed Mg^{2+}. Kanzaki et al. (2000) examined the role of Mg and Zn on the growth kinetics of hydroxylapatite. Both elements inhibited the lateral growth rate of 2-D nuclei on the {001} surface, with Zn affecting the growth rate approximatly 1000 times more than Mg. Supersaturation of hydroxylapatite was 22 in these solutions and Mg and Zn concentrations ranged from 0-1.5 mM and 0-7.5 μM respectively. It was concluded from AFM measurements and kinetic data fitted to adsorption models that the inhibitory affect of both Mg and Zn results from blocking of kink sites along steps of growth islands. Kanzaki et al. (2001) examined the affect of Mg and Zn sorption on the edge free energy and the rate of formation of 2-D nuclei. They found that it was negligible, although these impurities did block the lateral growth of 2-D nuclei. Brown (1981) found that the presence of both HCO_3 and Mg significantly decreased the rate of growth of hydroxylapatite. In these experiments the P-removal rate (used to indicate apatite growth rate) was approximately seven times faster at 1 mM HCO_3 than at 6 mM. In contrast, a 1 mM increase in Mg concentration in solution slowed P-removal by more than two orders of magnitude. Strontium was also found to inhibit the rates of both dissolution and growth of hydroxylapatite (Christoffersen et al. 1997). Two main mechanisms for the inhibition of apatite growth by impurity ions, exemplified in the previous studies, have been proposed: (1) impediment of the spreading of growth steps, and (2) poisoning of active growth sites or protosites. For cations a general trend of increasing inhibition with increasing charge has been observed (Mullin 1993). Wu and Nancollas (1998) derive expressions describing the influence of impurities on crystal growth kinetics based on their affect on surface free energy. Their model predicts increasing surface free energy with increasing charge of adsorbed foreign cations, with a commensurate increase in the growth inhibition with charge. It is interesting to note that a given impurity ion may have distinctly different effects on different phases. For example, while Mg strongly diminishes the growth rate of apatite it has a much smaller effect on the growth of OCP and DCPD (Nancollas and Zhang 1994). In general the kinetics of thermodynamically more stable phases are more sensitive to impurities in solution.

The influence of molecular species and extended polymers on apatite growth kinetics has also been investigated. Zieba et al. (1996) studied the kinetics of crystal growth of hydroxylapatite in the presence of seven different phosphonate additives. Their results indicate that traces of some phosphonates (less than or equal to 10^{-6} mol L^{-1}) are extremely effective in inhibiting crystal growth. Amjad and Reddy (1998) investigated the influence of seven humic compounds on the growth of hydroxylapatite. They found that fluvic acid, tannic acid, benzene hexacarboxylic acid, and poly(acrylic acid) had an inhibitory effect on growth, but salicyclic acid did not inhibit growth under the same experimental conditions (concentrations in solution between 0.25 and 5 ppm).

One of the major problems with using bulk solution data to determine growth mechanism is that the presence of impurities in solution, even at concentrations as low as

1 ppm, can significantly affect growth kinetics and have a profound affect on the processes involved in crystallization (Davey 1976, Wu and Nancollas 1998). Thus, interpretations based on growth rate theory of ideal systems can be in error. More accurate determination of growth mechanism is made by direct observations, either *in situ* or by inference based on certain types of surface microtopographic features.

DIRECT OBSERVATIONS OF GROWTH AT SURFACES

A second drawback with bulk solution studies of growth kinetics is that they yield an average of the kinetics of all the crystal faces. This leads to uncertainties in the estimation of surface properties determined from growth rate data, e.g., surface free energy. Indeed, on the basis of theory as well as limited direct measurements, we would expect that surface properties of symmetrically and structurally nonequivalent faces on the same crystal would be different. Because of symmetry constraints, apatite crystals will always be bound by at least two symmetrically nonequivalent forms, and as discussed previously, they may have many forms on a single crystal. Growth rate and mechanism may vary among different faces on the same crystal. To determine the mechanism of growth on any one face direct observations of growth or post-growth surface microtopography are needed.

Several studies have observed the growth mechanism *in situ* on specific crystal faces using atomic force microscopy (AFM). Using *in situ* AFM observations of growth on the {100} faces of synthetic hydroxylapatite, Onuma et al. (1995a) reported growth by step flow combined with two-dimensional nucleation. The rate-limiting step in growth was interpreted to be—based on step velocities—incorporation of growth units at the step fronts. They estimated the normal growth rate of the {100} face in their experiments to be on the order of 10^{-4} nm/s, on the basis of step advancement rates. In a similar study Onuma et al. (1995b) observed a hillock on {100} that advanced by a layer-spreading mechanism. The hillocks were anhedral and it was undetermined if they originated from a dislocation or 2-D nucleation. Using phase-shift interferometry and atomic force microscopy, Kanzaki et al. (1998) studied growth on the {001} face of a synthetic hydroxylapatite crystal in a simulated body fluid. Under the conditions of their experiments they found that growth took place by the formation of rounded islands of precipitate on the apatite surface, indicating a two-dimensional nucleation growth mode. They also found that the growth rate gradually decreased and eventually stopped, even though the solution chemistry was kept constant. The original growth rate was 1 to 2 orders of magnitude faster than that of on {100} determined by Onuma et al. (1995a). Onuma et al. (1998) investigated the growth rate dependence on supersaturation ($0.85 < S < 22.0$) by the same methods, and they estimate the edge free energy of a step on the {100} face to be 3.3 kT (k = Boltzmann constant). They also suggest that the critical supersaturation for growth to be 0.6. It is uncertain, however, if this is for spiral growth or two-dimensional nucleated growth.

Other studies have used *ex situ* observations of the surface microtopography of apatite to infer the growth mechanism in geologic samples. Growth spirals (Fig. 5) and hillocks (Figs. 6 and 7) on the {100} and {001} faces indicate that growth was by the spiral mechanism (Amelinckx 1952a,b; Rakovan and Reeder 1994, 1996). It is unclear, however, if polygonized growth hillocks can form by mechanisms other than spiral growth (Rakovan and Jaszczak 2002). For further discussion of these features, see the previous section on *Surface microtopography*.

IMPURITY INCORPORATION DURING GROWTH

The structure and composition of apatite lends itself to many compositional

substitutions; indeed, apatite incorporates over half the periodic table in its atomic arrangement (Hughes and Rakovan, Ch. 1, Pan and Fleet, Ch. 2 —both in this volume). These substitutions are usually in trace concentrations; however, complete solid solutions exist for certain substituents. This complex and variable chemistry has immense implications, and is utilized in all areas of apatite research, exemplified in many chapters in this volume.

Apatite can strongly influence the trace element evolution of magmas (e.g., Belousova et al. 2002). Many studies have shown apatite to be one of the most important minerals affecting rare earth element (REE) trends in igneous rocks (e.g., Nash 1972, Bergman 1979, Watson and Capobianco 1981, Kovalenko et al. 1982, Gromet and Silver 1983, Watson and Harrison 1984a,b), and volatile evolution in magmas (O'Reilly and Griffin 2000, Boudreau et al. 1986, Boudreau and McCallum 1989, Picolli and Candella, this volume). Thus, apatite chemistry can play a critical role in understanding and modeling of igneous petrogenetic processes (e.g., Papike et al. 1984, Sha and Chappell 1999, Spear and Pyle, Ch. 7, this volume; Picolli and Candella, Ch. 6, this volume). The formation of apatite in low-temperature sedimentary environments and from hydrothermal solutions can also strongly influence their trace element signature and evolution (e.g., Graf 1977, Bergman 1979, Watson and Capobianco 1981, McLennan 1989, Knudsen and Gunter, Ch. 9, this volume). Heavy metal sequestering by hydroxylapatite is important in our understanding of the fate and transport of toxic species in the body. The presence of certain elements in trace concentrations is also known to inhibit as well as promote apatite growth in the body (e.g., McLean and Bundy 1964, Posner 1987, Hahn 1989). Because of its affinity for many environmentally important elemental species, apatite is being used as an engineered contaminant barrier (i.e., Jeanjean et al. 1995, Chen et al. 1997, Arey et al. 1999, Seaman et al. 2001) for heavy metals and being investigated as a solid waste form for many radionuclides (Ewing 2001; Ewing, this volume). The presence of Mn and REEs in apatite gives it luminescence properties that are of great utility in both the phosphor and laser industries (e.g., McConnell 1973; Waychunas, this volume). Hence, knowledge of the variables that govern the partitioning of trace elements into apatite is of great importance.

Many complex variables affect the partitioning of trace elements into minerals during their formation. Trace element charge and size (Goldschmidt 1937), electro-negativity (Ringwood 1955), crystal field effects (Burns 1970), and crystal growth rate (Burton et al. 1953), as well as state variables such as temperature, pressure, and composition, have all been identified and studied as factors affecting trace element partitioning. More recently, the role of surface structure on the partitioning of elements into crystals has been demonstrated (Nakamura 1973, Dowty 1976, Reeder and Grams 1987, Paquette and Reeder 1990, Rakovan and Reeder 1994, Reeder and Rakovan 1999).

Surface structural controls on trace element incorporation during growth

***Compositional zoning*.** Studies of the incorporation of trace elements into apatite crystals that precipitated from hydrothermal solutions exemplify the role of crystal surface structure on heterogeneous reactivity. Rakovan and Reeder (1994) present cathodoluminescence (CL) and synchrotron X-ray fluorescence (SXRFMA) data that show heterogeneous incorporation of Y, Sr, Mn and REE into coeval regions of symmetrically different crystal faces (sectoral zoning). Differences in CL and photoluminescence (Waychunas, this volume) between different crystal faces can reveal sectoral zoning when luminescence-activating ions are differentially incorporated. Figure 15 shows the photoluminescence of an apatite crystal from Llallagua, Bolivia. The difference in luminescence color between {100}, orange, and {001}, lavender, indicates that the luminescence activators are segregated between these sets of crystal faces and

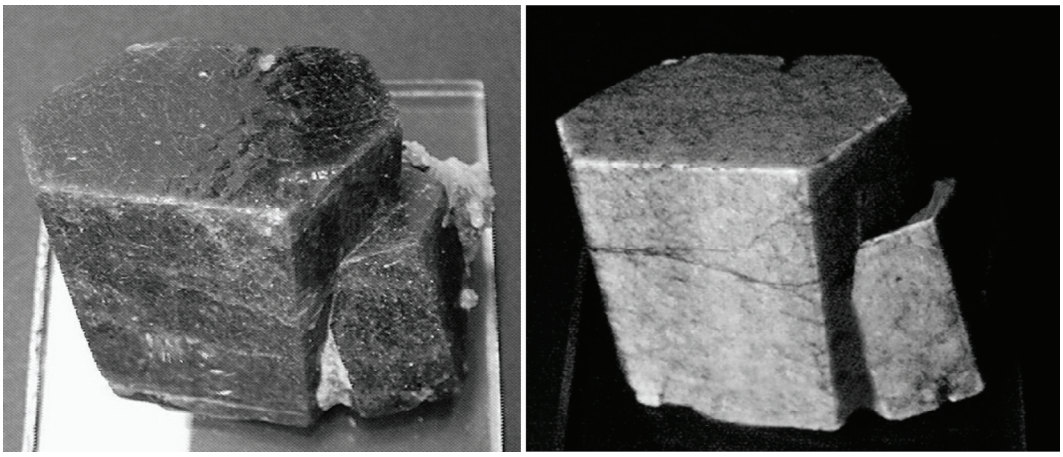

Figure 15. (*left*) Fluorapatite from the Siglo XX Mine, Llallagua, Bolivia. The larger crystal measures 3 × 3 × 2 cm. (*right*) Same, in long-wave ultraviolet light. Photoluminescence is activated by REEs. Differential luminescence between {001} faces, violet, and {100} faces, orange, indicates sectoral zoning REEs. See **Color Plate 1**, opposite page 718.

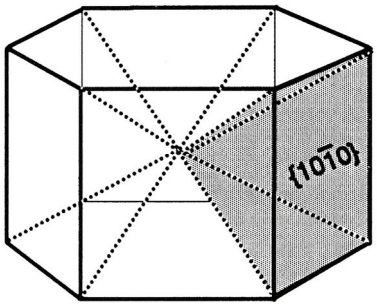

Figure 16. Diagram of a hexagonal apatite crystal showing the distribution of {100} and {001} sectors. One of the {100} prism sectors is shaded. [Modified after Rakovan and Reeder (1996).]

their associated sectors (Fig. 16) in the bulk crystal. Quantitative measurements, by isotope dilution mass spectrometry, of REE concentrations in coeval portions of {100} and {001} sectors of a Llallagua apatite (Fig. 17) show sectoral differences in concentration from roughly 1.4 for Yb to almost an order of magnitude (9.5) for La (Rakovan et al. 1997). One of the striking results of sectoral zoning of the REE, seen in Figure 17, is the significantly different REE patterns from different regions of the same crystal that grew simultaneously from the same fluid. Sectoral zoning of REE in the Llallagua apatite was used by Rakovan et al. (1997) for the development of an intracrystalline isochron dating technique (Fig. 18).

The {100} and {001} faces of the sectorally zoned apatites from Llallagua and numerous other locations exhibit polygonized growth hillocks (Figs. 6 and 7) that indicate a layer growth mechanism; most likely by spiral growth. In spiral growth, incorporation of constituent or substituent atoms takes place dominantly at kink sites along growth steps. Because of the symmetrical nonequivalence of {100} and {001}, the atomic structure of steps on those forms is different. Rakovan and Reeder (1994) suggested that this difference in the structure of surface sites of incorporation leads to a differential affinity for different trace elements and differential incorporation thereof, leading to sectoral zoning (Rakovan and Waychunas 1996, Rakovan et al. 1997).

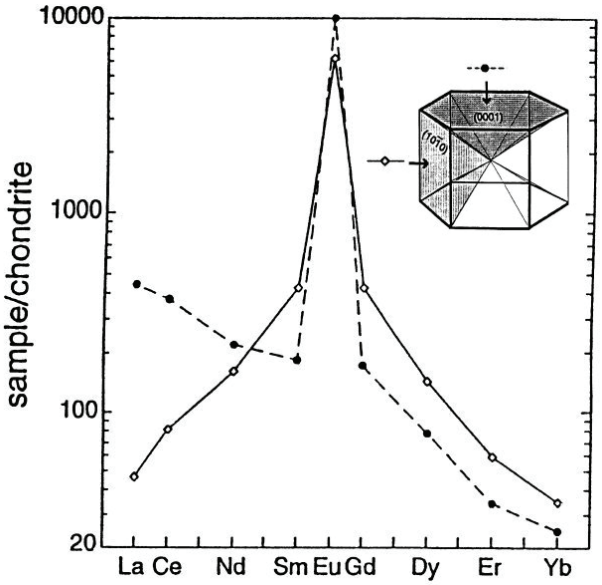

Figure 17. Chondrite-normalized REE patterns for coeval portions of {100} and {001} sectors of a single fluorapatite crystal from the Siglo XX Mine, Llallagua, Bolivia. Sectoral difference in the concentration of La is almost an order of magnitude. [Modified after Rakovan et al. (1997).]

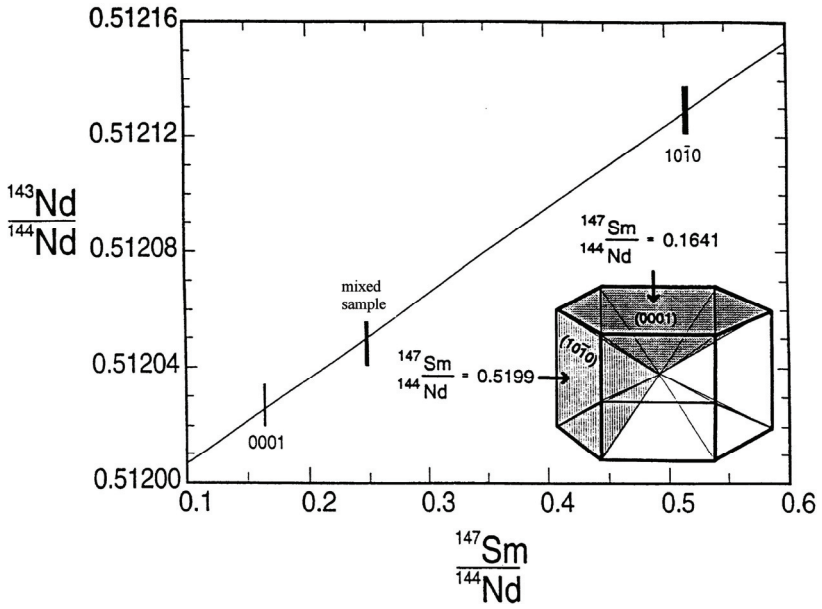

Figure 18. Sm-Nd isochron plot from coeval samples from different sectors of the sectorally zoned apatite in Figure 17. The isochron yields an age of crystallization of 43.8 ± 4.7 Ma. [Modified after Rakovan et al. 1997.]

Like sectoral zoning, intrasectoral zoning of trace elements in apatite also results from differential incorporation among structurally nonequivalent growth steps. In this case, however, the different steps reside on the same crystal face rather than different faces, and make up symmetrically nonequivalent vicinal faces of growth hillocks on the crystal face. Intrasectoral zoning, compositional differences between coeval portions of symmetrically different subsectors [regions of the bulk crystal that grew by incorporation

into a specific vicinal face of a growth hillock (Paquette and Reeder 1990)] was identified by Rakovan and Reeder (1994, 1996). Figure 19 shows the ideal subsector distribution for trigonal growth hillocks on {100} apatite faces. Intrasectoral differences in the distribution of luminescence-activating trace elements are clearly seen in cathodoluminescence (Figs. 20 and 21). Quantitative determination of REE concentration differences between the symmetrically nonequivalent subsectors by SXRFMA indicates that all of the REE, except for Eu, are intrasectorally zoned (e.g., Fig. 22). The partitioning behavior between subsectors associated with the nonequivalent growth steps was found to be correlated with the size of the REE ion relative to Ca^{2+}, the ion for which it substitutes in the apatite structure (Pan and Fleet, this volume); this indicates that substituent size was one of the main factors causing differential incorporation between nonequivalent surface sites. REEs with an ionic radius larger than Ca^{2+} (e.g., La^{3+}) are enriched in the [001] subsector relative to the <011> subsectors. All of the REEs analyzed that are smaller than Ca^{2+}, except Eu, are depleted in the [001] subsector relative to the <011>. A similar size affect is observed in sectoral zoning of REE between the {100} and {001} sectors in Llallagua apatites (Rakovan et al. 1997). The anomalous incorporation behavior of Eu can be explained by the fact that Eu is heterovalent in the Llallagua apatites (Fig. 23) (Rakovan et al. 2001a,b). In apatite, the ionic radius of Eu^{2+} is larger than Ca^{2+}, whereas Eu^{3+} is smaller. If Eu^{2+} follows the same partitioning behavior as the trivalent REEs that are larger than Ca, it will be enriched in the [001] subsector; the opposite is true of Eu^{3+}. Thus, roughly equal and opposite partitioning of the two ions between the nonequivalent sectors would yield the observed lack of intrasectoral zoning of total Eu.

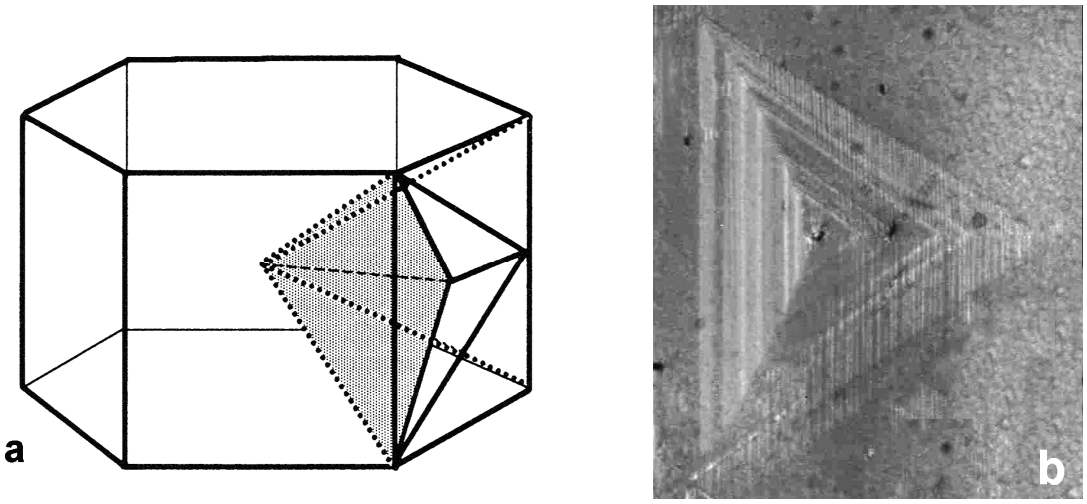

Figure 19. (a) Schematic of an apatite crystal with a three-sided growth hillock on a {100} face. The dotted lines indicate the sector associated with the prism face and the subsector of the basal vicinal face of the hillock is shaded. (b) A DIC photomicrograph of an actual hillock on the {100} face of a fluorapatite from the Golconda Mine, Minas Gerais, Brazil. Image is ~666 μm vertical. [Modified after Rakovan and Reeder (1996).]

The {001} faces of the Llallagua apatites studied by Rakovan and Reeder (1994) also exhibit growth hillocks, and associated subsectors display intrasectoral zoning. Six pyramidal vicinal faces and a terminating surface parallel to {001} form the hexagonal growth hillocks on the {001} faces. The face symmetry of {001} is a six-fold axis of rotation that symmetrically equates the <100> steps of all six pyramidal vicinal faces. CL of the six pyramidal vicinal faces of hillocks on the {001} of Llallagua apatite crystals is homogenous, as expected on the basis of their symmetry equivalence. Differential

incorporation, however, does take place between the pyramidal vicinal faces and the {001} terminations and regions of the {001} surface where no hillocks are present (Fig. 24, and cover). The exact mechanism of this intrasectoral zoning is uncertain (Rakovan and Reeder 1994).

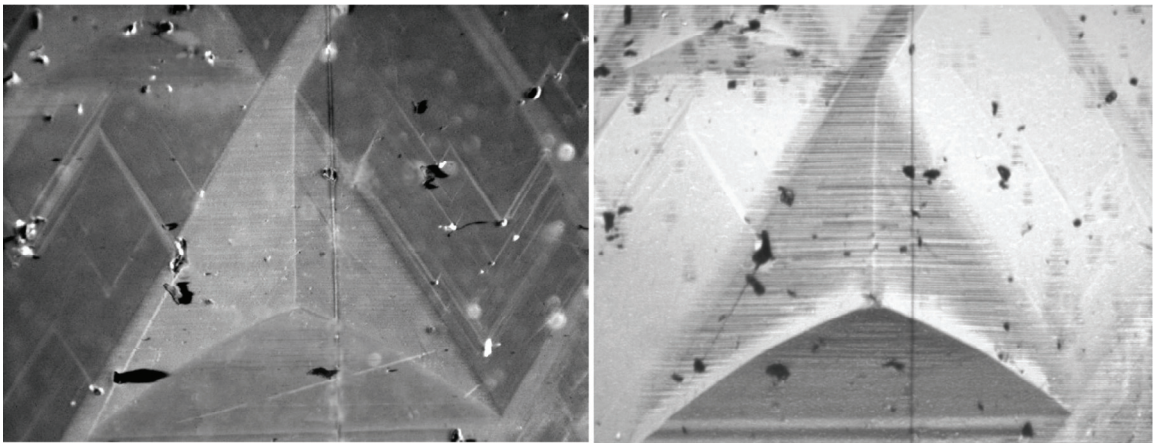

Figure 20. (*left*) Cathodoluminescence (REE activated) photomicrograph of the growth hillock in right image. Luminescence is homogenous between the two symmetrically equivalent vicinal faces (color is orange). Differential luminescence exists between these and the symmetrically nonequivalent vicinal face, whose luminescence is blue. See **Color Plate 2**, opposite page 718. (*right*) DIC photomicrograph of a trigonal growth hillock on the {100} face of a fluorapatite from the Golconda Mine, Minas Gerais, Brazil. Image is ~1 mm across. [Used by permission of the Mineralogical Society of America, from Rakovan and Reeder (1994) *American Mineralogist*, Vol. 79, Fig. 6, p. 897.]

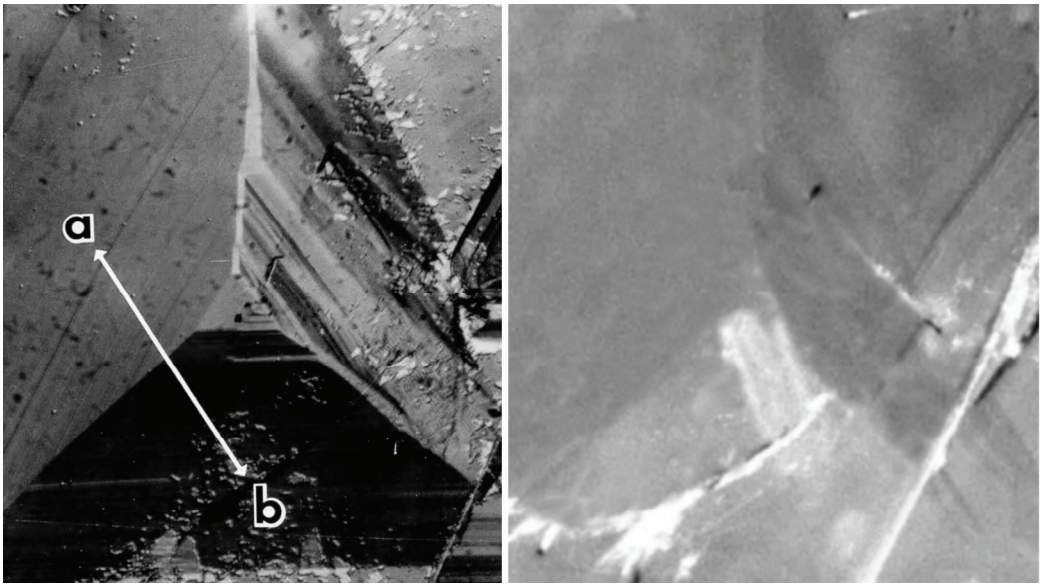

Figure 21. (*left*) DIC photomicrograph of a trigonal growth hillock on the {100} face of a fluorapatite from the Siglo XX Mine, Llallagua, Bolivia. Steps of $[01\bar{1}]$ orientation comprise vicinal face **a**, and steps of [001] orientation comprise vicinal face **b**. Image is ~2.4 mm across. (*right*) Cathodoluminescence photomicrograph of the hillock in left image. Luminescence is homogenous between the two symmetrically equivalent vicinal faces (yellow luminescence activated by Mn^{2+}). Differential luminescence exists between these and the symmetrically nonequivalent vicinal face, whose luminescence is blue (activated by REE). See **Color Plate 3**, opposite page 718. [Modified after Rakovan and Reeder (1996).]

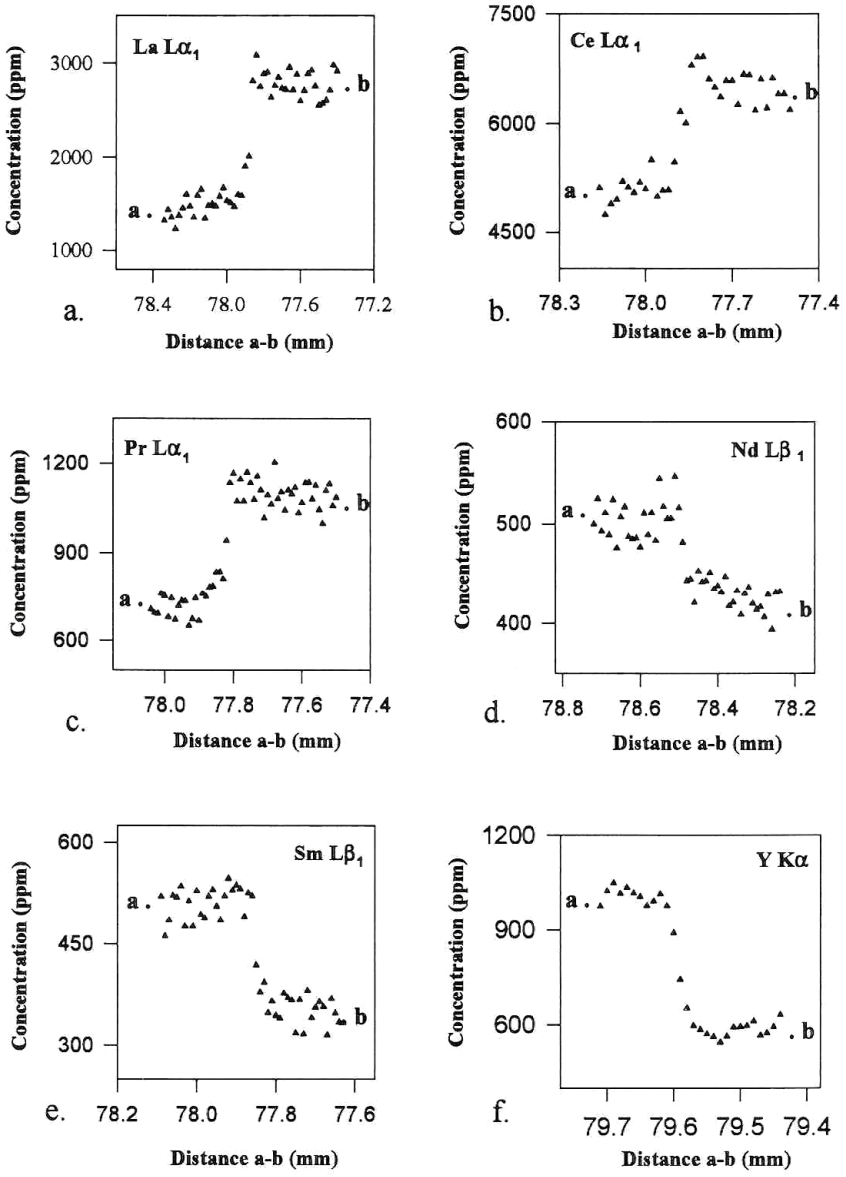

Figure 22. Plots of the concentration of selected REEs between symmetrically nonequivalent vicinal faces, and their associated subsectors, along the line *a-b* shown in Figure 21a. [Used by permission of Elsevier Science Ltd., from Rakovan and Reeder (1996) *Geochimica et Cosmochimica Acta*, Vol. 60, Fig. 3, p. 4439.]

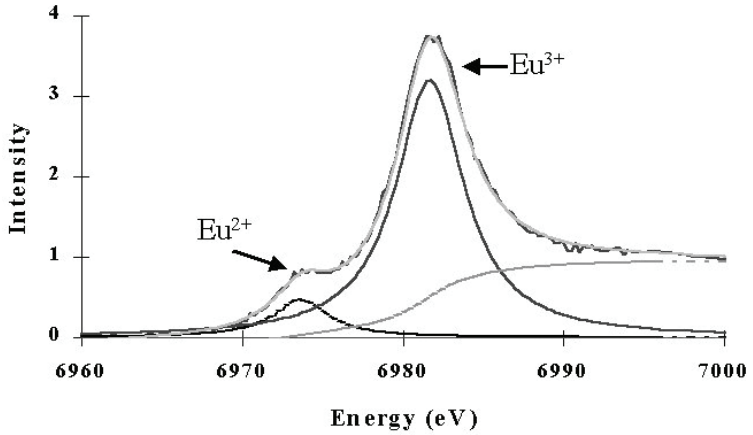

Figure 23. Eu L3-edge XANES data for the Llallagua apatite indicating the presence of heterovalent europium. [Used by permission of the Mineralogical Society of America, from Rakovan and Reeder (2001) *American Mineralogist*, Vol. 86, Fig. 3, p. 699.]

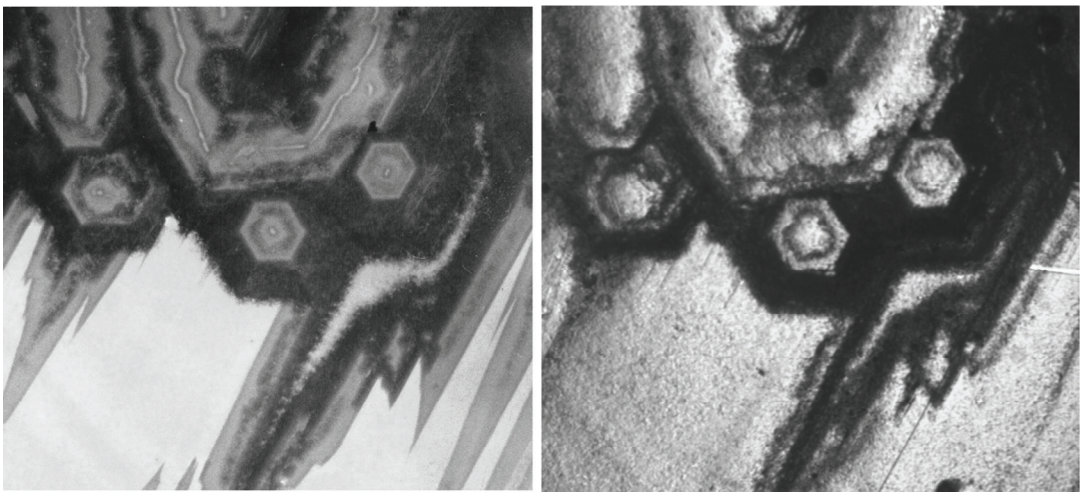

Figure 24. (*left*) Cathodoluminescence photomicrograph of hexagonal growth hillocks on the {001} face of an apatite from the Siglo XX Mine, Llallagua, Bolivia. Luminescence (purple, activated by REEs) is homogenous among the six symmetrically equivalent pyramidal vicinal faces. Yellow luminescence (Mn^{2+} activated) dominates flat regions of the {001} face and the terminal faces of the hillocks. See cover or **Color Plate 4**, opposite page 718. (*right*) DIC photomicrograph showing the microtopography of the {001} apatite face in left image. Image is ~1.2 mm across. [Used by permission of the Mineralogical Society of America, from Rakovan and Reeder (1994) *American Mineralogist*, Vol. 79, Fig. 7, p. 897.]

Superposition of sectoral, intrasectoral, and concentric zoning can lead to complex trace element distribution patterns within single crystals that may be difficult to interpret in randomly-oriented crystal sections. Several authors (i.e., Marshall 1988, Jolliff et al. 1989) have noted a clustering or patchy distribution of REE within individual crystals of apatite. Several explanations have been given, but it is quite possible that such anomalous distributions are due to intrasectoral or sectoral zoning. Kempe and Gotze (2002) identified concentric and sectoral zoning in oriented sections of apatite crystals (Figs. 25 and 26). The polygonized domains of different luminescence intensity within single sectors in Figure 25 may be subsectors indicating intrasectoral zoning as well.

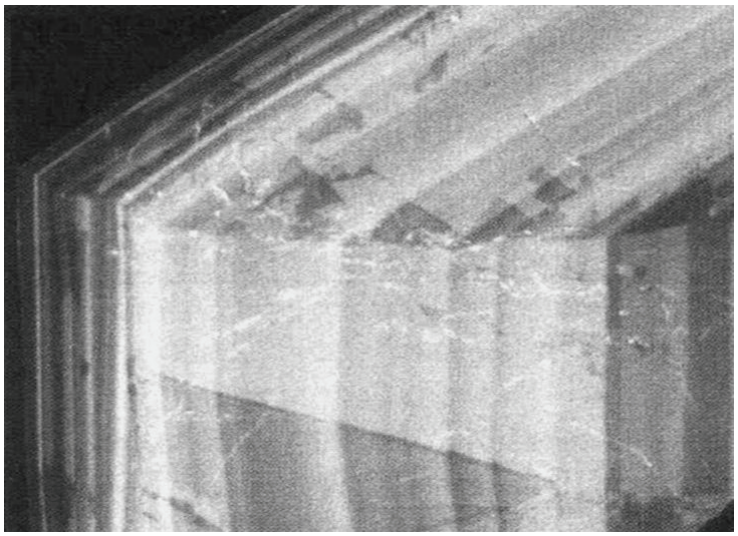

Figure 25. Cathodoluminescence photomicrograph of a section cut through an apatite from Ehrenfriedersdorf, Germany, exhibiting concentric, sectoral and intrasectoral zoning. Yellow luminescence activated by Mn^{2+}. [Used by permission of the Mineralogical Society, from Kempe and Götze (2002) *Mineralogical Magazine*, Vol. 66, Fig. 2e, p. 156.]

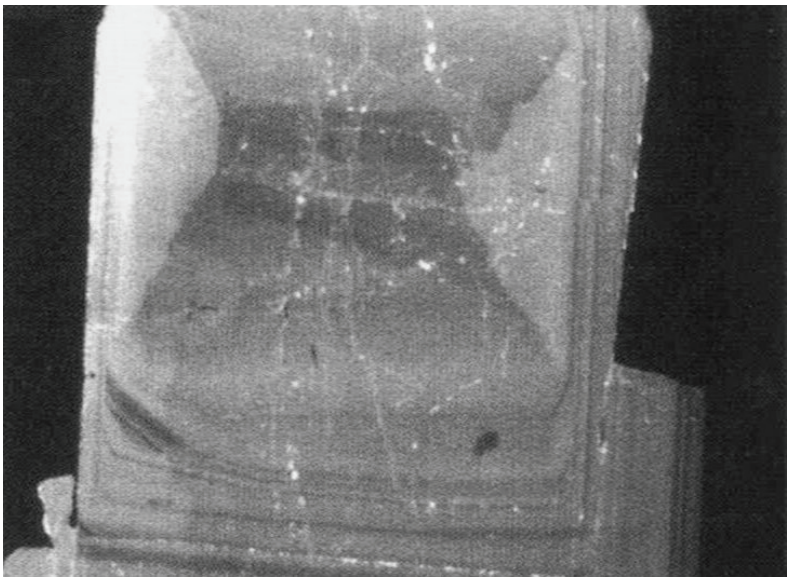

Figure 26. Cathodoluminescence photomicrograph of a section cut through an apatite from Ehrenfriedersdorf, Germany exhibiting oscillatory and sectoral zoning. Yellow luminescence activated by Mn^{2+}. [Used by permission of the Mineralogical Society, from Kempe and Götze (2002) *Mineralogical Magazine*, Vol. 66, Fig. 2f, p. 156].

Surface-induced dissymmetrization. Akizuki et al. (1994) and Rakovan and Reeder (1994) reported optical anomalies in apatite crystals from the Asio Mine, Japan, and Llallagua, Bolivia, respectively. In both cases the apatite crystals exhibit concentric, sectoral and intrasectoral domains with different optical orientation and character. The correlation of these domains with surface features, such as specific crystal faces, indicates that the optical anomalies were created during growth of the crystals. There are several possible causes for the optically anomalous behavior. Certain anomalies may be the result of inhomogeneous mismatch strain from impurities. It has also been shown that the type of surface structural control on element incorporation that leads to compositional sectoral and intrasectoral zoning can also cause ordering and a lowering of crystal symmetry (dissymmetrization) during growth (Bulka et al. 1980, Akizuki 1987, Akizuki and Sunagawa 1978, Shtukenberg et al. 2001).

In the apatites from Japan, Akizuki et al. (1994) found biaxial optical character with domains of different optical orientation and $2V$ (Fig. 27). Although the optical properties indicate a monoclinic or triclinic structure, electron and X-ray diffraction data showed no reflections inconsistent with $P6_3/m$ symmetry or that indicate a superstructure. They postulated that the dissymmetrization is due to ordering of OH and F (Hughes and Rakovan, this volume) along growth steps during incorporation.

In the Llallagua apatites, {001} sectors with two different optical characters have been found from different parts of the mine. The {001} sectors are typically uniaxial negative, as would be expected for $P6_3/m$ apatite. However, in some crystals (i.e., those in Figs 7 and 15) the {001} sector is optically biaxial and sub-sectoral domains associated with the pyramidal vicinal faces of hexagonal hillocks on the {001} faces show different optical orientation (Fig. 28). In all of the Llallagua samples studied, {101}, {111} and {100} sectors show biaxial character with distinct concentric and sectoral zoning of extinction orientation and $2V$. Coeval portions of a given sector, as indicated by a single continuous concentric zone, show subsector differences in $2V$ from 2° to as much as 15° (Fig. 29). Rakovan and Reeder (1994) also postulated that the

optical anomalies in these crystals were due to ordering during growth, potentially of F and OH ions. Less complex, but distinctly different, are optically anomalous apatites reported by Richards and Rakovan (2000). These crystals show single biaxial domains that correlate with the six {100} sectors of tabular crystals (Fig. 30).

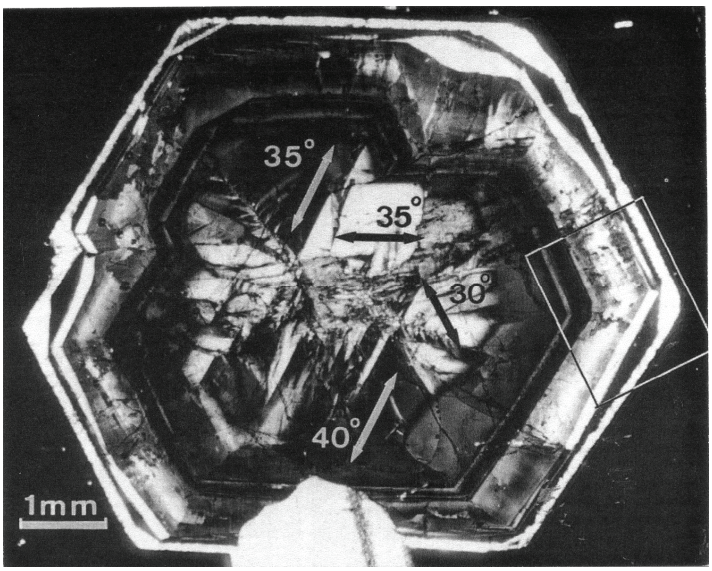

Figure 27. Optical photomicrograph in crossed polarized transmitted light of a thin section (parallel to {001}) through an apatite from the Asio Mine, Shimotsuke Province, Japan. Optically distinct regions correspond to different sectors and subsectors throughout the crystal. [Used by permission of the Mineralogical Society, from Akizuki et al. (1994) *Mineralogical Magazine*, Vol. 58, Fig. 4, p. 311.]

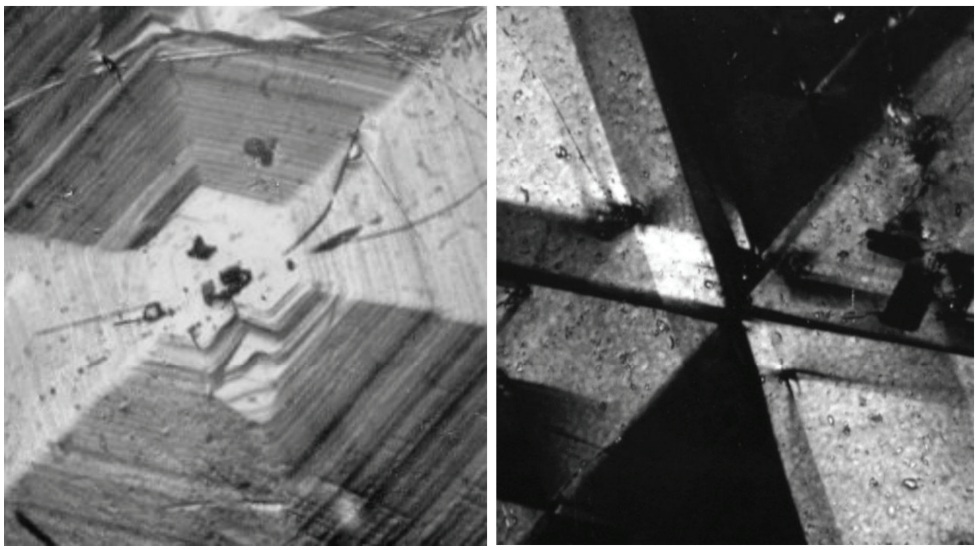

Figure 28. (*left*) DIC photomicrograph of a hexagonal growth hillock on a {001} face of an apatite from the Siglo XX Mine, Llallagua, Bolivia (see Fig. 7). Image is ~1.2 mm across. (*right*) Optical photomicrograph of a thin section (parallel to {001} within a {001} sector) in crossed polarized transmitted light. Optically-distinct regions correspond to the different subsectors beneath the vicinal faces of the growth hillock in a.

Studies of surface structural controls on trace element incorporation into apatite and other minerals during growth exemplify that a bulk crystallographic site may have multiple, distinctly different surface representations (surface sites). Differences between these surface sites may lead to heterogeneous reactivity at the mineral-water interface (Reeder and Rakovan 1999). Sectoral and intrasectoral zoning in apatite demonstrates nonequilibrium incorporation and that factors such as growth mechanism and surface structure are important in trace element partitioning. Furthermore, these zoning types

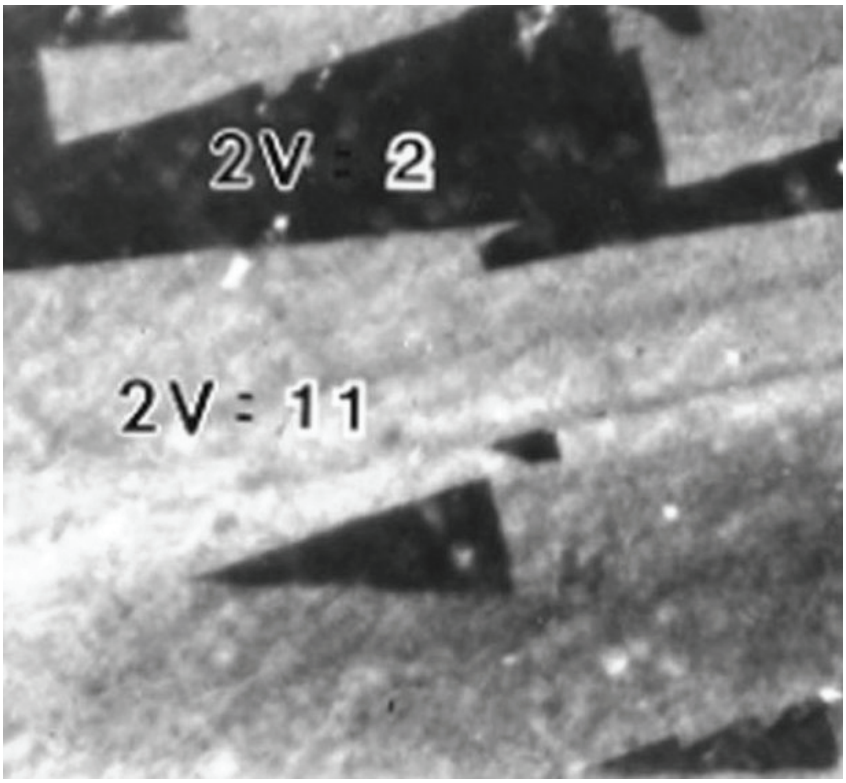

Figure 29. Optical photomicrograph of a thin section (parallel to {001} within a {100} sector) in crossed polarized transmitted light; from the same apatite crystal in Figure 28. Optically-distinct regions correspond to the different concentric zones and subsectors within the {100} sector. Image is ~500 μm across.

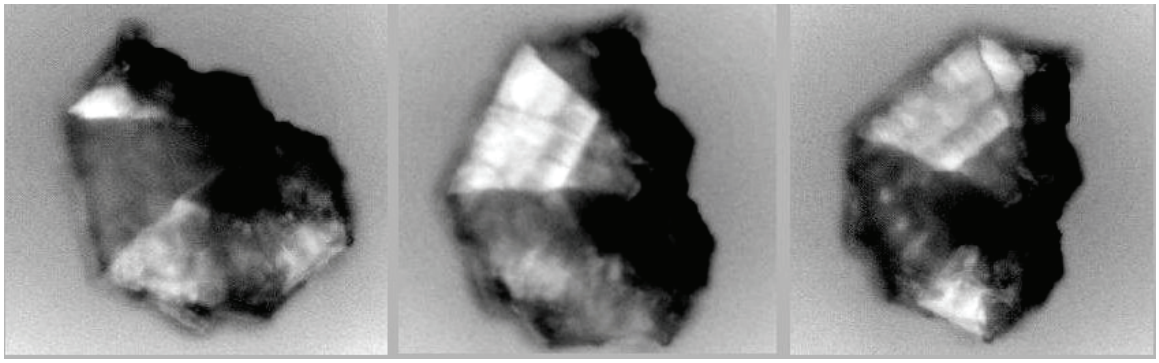

Figure 30. Optical photomicrographs in crossed polarized transmitted light of an apatite in three different orientations from Huron County, Ohio, United States. The optical path is parallel to [001]. Optically distinct regions correspond to the different {100} sectors. The crystal is ~2 mm across.

suggest that partition coefficients, K_d, for a given mineral-fluid system are not unique; rather, the K_d may differ for structurally distinct regions of a crystal surface. Ultimately, this bears on the use of trace element concentrations in minerals as indicators of petrogenetic processes in all types of rock forming environments where apatite is found. Surface structure not only plays an important role in differential partitioning of trace elements into apatite during growth but also influences ordering of atoms, leading to dissymmetrization.

CONCLUSIONS

The nature of the apatite surface, particularly as it exists in contact with complex aqueous solutions, and the processes involved in apatite crystal growth and trace element incorporation have been studied extensively. However the apatite surface and mechanisms of growth are very complex and many questions about the structure of active surface sites of adsorption and incorporation, the free energies of different crystal faces and growth steps, controlling factors on morphology and surface microtopography, mechanisms of impurity affects on growth, and the relationships between differential incorporation leading to compositional zoning and dissymmetrization remain outstanding.

In studies of crystals growth, microtopographic features such as growth spirals are well understood and can be used as indicators of growth mechanisms and to some extent growth conditions. Other commonly observed microtopographic features are not so well understood. Likewise, controls on the morphology and specific face development of apatite are poorly understood. A better understanding of the controls on morphologic and surface microtopographic features, and variations there of, will allow scientists to more widely use these features on natural samples to unravel information about the crystallization and post crystallization histories of biologic and geologic apatites.

The formation of precursor phases, the strong influence of impurity species, and the face specific and step specific incorporation of trace elements all point to kinetic and mechanistic factors being particularly important in the crystal growth of apatite from solution. Surface structural and chemical affects clearly may be more important than thermodynamics in driving crystallization processes of apatite at low temperatures. This is especially true in biological and geological systems where complex environments contain many different impurities, from single ions to complex organic molecules and polymers. The role of precursor phases in the formation of apatite in low temperature geologic environments is poorly understood. This is of particular significance in understanding the role of apatite on the fate of environmentally significant species such as heavy metals and radionuclides.

With the rapid advances in nanotechnology, including new methods for direct observation and analysis of surfaces at the nanometer and atomic scales, more insights pertaining to these and other unanswered questions will be made.

ACKNOWLEDGMENTS

I thank Rich Reeder, John Jaszczak and John Hughes for their reviews of this chapter. I also thank Chris Thomas for his help in editing this chapter and many others in this volume.

REFERENCES

Akizuki M, Sunagawa I. (1978) Study of the sector structure in adularia by means of optical microscopy, infra-red absorption, and electron microscopy. Mineral Mag 42:453-462

Akizuki M (1987) Crystal symmetry and order-disorder structure of brewsterite. Am Mineral 72:645-648

Akizuki M, Nisidoh H, Kudoh Y, Watanabe T, Kurata K (1994) Sector growth and symmetry of (F,OH) apatite from the Asio mine, Japan. Mineral Mag 58:307-314

Amelinckx S (1952a) Spiral growth patterns on apatite crystals. Nature 169:841-842

Amelinckx S (1952b) Growth spirals and their relation to crystal habit as illustrated by apatite. Nature 170:760-761

Amjad Z, Koutsoukos PG, Nancollas GH (1981) The crystallization of fluorapatite: A constant-composition study. J Colloid Inter Sci 82:394-400

Amjad Z, Reddy MM (1998) Influence of humic compounds on the crystal growth of hydroxylapatite. *In* Water Soluble Polymers. Amjad Z (ed) Plenum Press, New York

Arends J, Christoffersen J, Christoffersen MR, Eckert H, Fowler BO, Heughebaert JC, Nancollas GH, Yesinowski JP, Zawacki SJ (1987) A calcium hydroxylapatite precipitated from an aqueous-solution—an international multimethod analysis. J Cryst Growth 84:515-532

Arey JS, Seaman JC, Bertsch PM (1999) Immobilization of uranium in contaminated sediments by hydroxyapatite addition. Environ Sci Tech 33:337-342

Belousova EA, Griffin WL, O'Reilly SY, Fisher NI. (2002) Apatite as an indicator mineral for mineral exploration: Trace-element compositions and their relationship to host rock type. J Geochem Explor 76:45-69

Bergman SC (1979) The significance of accessory apatite in the REE modeling of magma genesis. EOS Trans Am Geophys Union 60:412

Boistelle R, Astier JP (1988) Crystallization mechanisms in solution. J Cryst Growth 90:14-30

Boskey AL, Posner AS (1973) Conversion of amorphous calcium phosphate to microcrystalline hydroxyl-apatite. A pH-dependent, solution-mediated, solid-solid conversion. J Phys Chem 77: 2313-2317

Boskey AL, Posner AS (1976) Formation of hydroxylapatite at low supersaturation. J Phys Chem 80:40-45

Boudreau AE, Mathez EA, Mccallum IS (1986) Halogen geochemistry of the Stillwater and Bushveld complexes—Evidence for transport of the platinum-group elements by Cl-rich fluids. J Petrol 27: 967-986

Boudreau AE, McCallum IS (1989) Investigations of the Stillwater Complex; Part 5, Apatites as indicators of evolving fluid composition. Contrib Mineral Petrol 102:138-153

Brecevic LJ, Furedi-Milhofer H (1972) Precipitation of calcium phosphates from electrolyte solutions II: The formation and transformation of the precipitates. Calc Tissue Res 10:82-90

Brown WE (1966) Crystal Growth of Bone Mineral. Clin Orthopaed 44:205-220

Brown JL (1981) Calcium phosphate precipitation: Effects of common and foreign ions on hydroxyapatite crystal growth. Soil Sci Soc J 45:482-486

Bulka GR, Vinokurov VM, Nizamutdinov NM, Hasanova NM (1980) Dissymmetrization of crystals: Theory and experiment. Phys Chem Minerals 6:283-293

Burns RG (1970) Mineralogical Applications of Crystal Field Theory. Cambridge University Press, Cambridge

Burton JA, Prim RC, Slichter WP (1953) The distribution of solute in crystals grown from the melt. Part I: Theoretical. J Chem Phys 21:1987-1991

Burton WK, Cabrera N, Frank FC (1951) The Growth of Crystals and the Equilibrium Structure of their Surfaces. Phil Trans 243:299-358

Busscher HJ, De Jong HP, Arends J (1987) Surface free energies of hydroxylapatite, fluorapatite and calcium fluoride. Mater Chem Phys 17:553-558

Chander S, Fuerstenau DW (1984) Solubility and interfacial properties of hydroxylapatite: A review. *In* Adsorption On and Surface Chemistry of Hydroxyapatite. Misra DN (ed) Plenum Press, New York

Chen XB, Wright JV, Conca JL, Peurrung LM (1997) Evaluation of heavy metal remediation using mineral apatite. Water Air Soil Poll 98:57-78

Chin KOA, Nancollas GH (1991) Dissolution of fluorapatite—A constant-composition kinetics study. Langmuir 7:2175-2179

Christoffersen J, Christoffersen MR, Kibalczyc W, Andersen FA (1989) A contribution to the under-standing of the formation of calcium phosphates. J Cryst Growth 94:767-777

Christoffersen J, Landis WJ (1991) A contribution with review to the description of mineralization of bone and other calcified tissues *in vivo*. Anatom Rec 230:435-450

Christoffersen J, Rostrup E, Christoffersen MR (1991) Relation between interfacial surface-tension of electrolyte crystals in aqueous suspension and their solubility—A simple derivation based on surface nucleation. J Cryst Growth 113:599-605

Christoffersen J, Christoffersen, MR (1992a) A revised theory for the growth of crystals by surface nucleation. J Cryst Growth 121:608-616

Christoffersen MR, Christoffersen J (1992b) Possible mechanisms for the growth of the biomaterial, calcium hydroxylapatite microcrystals. J Cryst Growth 121:617-630

Christoffersen J, Christoffersen MR, Johansen T (1996a) Kinetics of growth and dissolution of fluorapatite. J Cryst Growth 163:295-303

Christoffersen J, Christoffersen MR, Johansen T (1996b) Some new aspects of surface nucleation applied to the growth and dissolution of fluorapatite and hydroxylapatite. J Cryst Growth 163:304-310

Christoffersen J, Christoffersen MR, Kolthoff N, Barenholdt O (1997) Effects of strontium ions on growth and dissolution of hydroxyapatite and on bone mineral detection. Bone 20:47-54

Christoffersen J, Dohrup J, Christoffersen MR (1998a) The importance of formation of hydroxyl ions by dissociation of trapped water molecules for growth of calcium hydroxylapatite crystals. J Cryst Growth 186:275-282

Christoffersen MR, Dohrup J, Christoffersen J (1998b) Kinetics of growth and dissolution of calcium hydroxylapatite in suspensions with variable calcium to phosphate ratio. J Cryst Growth 186:283-290
Davey RJ (1976) The effect of impurity adsorption on the kinetics of crystal growth from solution. J Cryst Growth 34:109-19
Davies CW (1962) Ion Association. Butterworths, London
Deutsch Y, Sarig S (1977) The effect of fluoride ion concentration on apatite formation and on its crystal habit. J Cryst Growth 42:234-237
Dowty E. (1976) Crystal structure and crystal growth II: Sector zoning in minerals. Am Mineral 61:460-469
Driessens FCM (1982) Mineral Aspects of Dentistry. S. Karger, Basel
Eanes ED, Gillessen IH, Posner AS (1966) Mechanism of conversion of non-crystalline calcium phosphate to crystalline hydroxylapatite. *In* Crystal Growth. Peiser HS (ed) Pergamon Press, Oxford
Elliott JC (1994) Structure and Chemistry of the Apatites and Other Calcium Orthophosphates. Elsevier, Amsterdam
Ewing RC (2001) The design and evaluation of nuclear-waste forms: clues from mineralogy. Can Mineral 39:697-715
Feenstra TP, Bruyn PLD (1979) Formation of calcium phosphates in moderately supersaturated solutions. J Phys Chem 83:475-479
Francis MD, Web NC (1971) Hydroxylapatite formation from hydrated calcium monohydrogen phosphate precursor. Calc Tissue Res 6:335-342
Gilmer GH (1976) Growth on imperfect crystal faces I. Monte-Carlo growth rates. J Cryst Growth 35: 15-28
Gilmer GH, Jackson KA (1977) Computer simulation of crystal growth. *In* Current Topics in Materials Science. Vol 2. Kaldis E, Scheel HJ (eds) North-Holland Pub, Amsterdam
Goldschmidt VM (1913) Atlas der Kristallformen. Heidelberg
Goldschmidt VM (1937) The principles of distribution of chemical elements in minerals and rocks. J Chem Soc London, p 655-673
Graf JL (1977) Rare earth elements as hydrothermal tracers during the formation of massive sulfide deposits in volcanic rocks Appears. Econ Geol 72:527-548
Gromet, L.P., and Silver L.T. (1983) Rare earth element distributions among minerals in a granodiorite and their petrologic implications. Geochim Cosmochim Acta 47:952-938
Hahn TJ (1989) Aluminum-related disorders of bone and mineral metabolism. *In* Bone and Mineral Research Vol. 6. Peck WA (ed) Elsevier, New York
Hartman P, Perdok WG (1955a) On the relations between structure and morphology of crystals. I. Acta Crystallogr 8:49-52
Hartman P, Perdok WG (1955b) On the relations between structure and morphology of crystals. II. Acta Crystallogr 8:521-529
Hillig WB (1966) A derivation of classical two-dimensional nucleation kinetics and the associated crystal growth laws. Acta Metall 14:1868-1969
Hochella MF, White AF (eds) (1990) Mineral-Water Interface Geochemistry—an Overview. Rev Mineral 23. Mineralogical Society of America, Washington, DC
Hogarth DD (1974) The discovery of apatite on the Lièvre River, Quebec. Mineral Rec 5:178-182
Hohl H, Koutsoukos PG, Nancollas GH (1982) The crystallization of hydroxylapatite and dicalcium phosphate dihydrate; representation of growth curves. J Cryst Growth 57:325-35
Inskeep WP, and Silvertooth JC (1988) Kinetics of hydroxylapatite precipitation at pH 7.4 to 8.4. Geochim Cosmochim Acta 52:1883-1893
Jaynes WF, Moore PA Jr., Miller DM (1999) Solubility and ion activity products of calcium phosphate minerals. J Environ Qual 28:530-536
Jeanjean J, Rouchaud JC, Tran L, Fedoroff M (1995) Sorption of uranium and other heavy metals on hydroxyapatite. J Radioanal Nuclear Chem Lett 201:529-539
Jolliff BL, Papike JJ, Shearer CK, Shimizu N (1989) Inter- and intra-crystal REE variations in apatite from the Bob Ingersoll pegmatite, Black Hills, South Dakota. Geochim Cosmochim Acta 53:429-441
Kanzaki N, Onuma K, Ito A, Teraoka, K, Tateishi T, Tsutsumi S (1998) Direct growth rate measurement of hydroxylapatite single crystal by Moire phase shift interferometry. J Phys Chem B 102:6471-6476
Kanzaki N, Onuma K, Treboux G, Tsutsumi S, Ito A (2000) Inhibitory effect of magnesium and zinc on crystallization kinetics of hydroxylapatite (0001) face. J Phys Chem B 104:4189-4194
Kanzaki N, Onuma K, Treboux G, Tsutsumi S, Ito A (2001) Effect of impurity on two-dimensional nucleation kinetics: Case studies of magnesium and zinc on hydroxylapatite (0001) face. J Phys Chem B 105:1991-1994
Kempe U, Gotze J (2002) Cathodoluminescence (CL) behaviour and crystal chemistry of apatite from rare-metal deposits. Mineral Mag 66:151-172

Kostov I, Kostov RI (1999) Crystal Habits of Minerals. Pensoft Publisher, Sofia
Koutsopoulos S (2001) Kinetic study on the crystal growth of hydroxylapatite. Langmuir 17:8092-8097
Koutsoukos P, Amjad Z, Tomson MB, Nancollas GH (1980) Crystallization of calcium phosphates—Constant-composition study. J Am Chem Soc 102:1553-1557
Kovalenko VI, Antipin VS, Vladykin NV, Smirnova YV, Balashov YA (1982) Rare-earth distribution coefficients in apatite and behavior in magmatic processes. Geokhimiya 2:230-242
Lindsay (1979) Chemical Equilibria in Soils. Wiley Interscience, New York
Liu Y, Nancollas GH (1996) Fluorapatite growth kinetics and the influence of solution composition. J Cryst Growth 165:116-123
Lundager-Madsen HE, Christensson F (1991) Precipitation of calcium phosphate at 40 degrees C from neutral solution. J Cryst Growth 114:613-18
Marshall DJ (1988) Cathodoluminescence of Geological Materials. Unwin Hyman, Boston
McLean FC, Bundy AM (1964) Radiation, Isotopes, and Bone. Academic Press, New York
McLennan SM (1989) Rare earth elements in sedimentary rocks: Influence of provenance and sedimentary processes. Rev Mineral 21:169-200
McConnell D (1973) Apatite: Its Crystal Chemistry, Mineralogy, Utilization and Geologic and Biologic Occurrences. Springer Verlag, New York
Moreno EC, Varughese K (1981) Crystal growth of calcium apatites from dilute solutions. J Cryst Growth 53:20-30
Müller-Krumbhaar H, Burkhard TW, Kroll D (1977) A generalized kinetic equation for crystal growth. J Cryst Growth 38:13-22
Mullin JW (1993) Crystallization. Butterworth-Heinemann Ltd., London
Nakamura Y (1973) Origin of sector zoning in igneous clinopyroxenes. Am Mineral 58:986-990
Nancollas GH, Tomazic B (1974) Growth of calcium phosphate on hydroxylapatite crystals. Effect of supersaturation and ionic medium. J Phys Chem 78:2218-2225
Nancollas GH (1979) The growth of crystals in solution. Adv Colloid Inter Sci 10:215-52
Nancollas GH (1982) Phase transformation during precipitation of calcium salts. *In* Biological Mineralization and Demineralization. Nancollas GH (ed) Springer-Verlag, Berlin, p 79-99
Nancollas GH (1984) The nucleation and growth of phosphate minerals. *In* Phosphate Minerals: Their Properties and General Modes of Occurrence. Nriagu JO, Moore PB (eds) Springer-Verlag, Berlin
Nancollas GH, Zhang J (1994) Formation and dissolution mechanisms of calcium phosphates in aqueous systems. *In* Hydroxylapatite and Related Materials. CRC Press, Boca Raton, Florida
Nash WP (1972) Apatite chemistry and phosphorus fugacity in a differentiated igneous intrusion. Am Mineral 57:877-886
Nielsen AE (1984) Electrolyte crystal growth mechanisms. J Cryst Growth 67:289-310
Nielsen AE, Toft JM (1984) Electrolyte crystal growth kinetics. J Cryst Growth 67:278-288
Nylen MU, Eanes ED, Omnell KA (1963) Crystal Growth in Rat Enamel. J Cell Biol 18:109-123
Onuma K, Ito A, Tateishi T, Kameyama T (1995a) Growth kinetics of hydroxylapatite crystal revealed by atomic force microscopy. J Cryst Growth 154:118-125
Onuma K, Ito A, Tateishi T, Kameyama T (1995b) Surface observations of synthetic hydroxylapatite single crystal by atomic force microscopy. J Cryst Growth 148:201-206
Onuma K, Kanzaki N, Ito A, Tateishi T (1998) Growth kinetics of the hydroxylapatite (0001) face revealed by phase shift interferometry and atomic force microscopy. J Phys Chem B 102:7833-7838
O'Reilly SY, Griffin WL (2000)Apatite in the mantle: Implications for metasomatic processes and high heat production in Phanerozoic mantle. Lithos 53:217-232
Palache C, Berman H, Frondel C (1951) The system of mineralogy of James Dwight Dana and Edward Salisbury Dana. Wiley and Sons, London
Papike JJ, Jensen M, Laul JC, Shearer CK, Simon SB, Walker RJ (1984) Apatite as a recorder of pegmatite petrogenesis. Geol Soc Am Abstr Progr 16:617
Paquette J, Reeder RJ (1990) A new type of compositional zoning in calcite: Insights into crystal-growth mechanisms. Geology 18:1244-1247
Paquette J, Reeder RJ (1995) Relationship between surface structure, growth mechanism, and trace element incorporation in calcite. Geochim Cosmochim Acta 59:735-751
Phakey PP, Leonard JR (1970) Dislocations and fault surfaces in natural apatite. J Appl Crystallogr 3:38-44
Pina C, Becker U, Risthaus P, Bosbach D, Putnis A (1998) Molecular-scale mechanisms of crystal growth in barite. Nature 395:483-486
Posner A.S. (1987) Bone Mineral and the Mineralization Process. Bone Mineral Res Vol. 5. Peck WA (ed) Elsevier, New York
Rakovan J, Reeder RJ (1994) Differential incorporation of trace-elements and dissymmetrization in apatite—The role of surface-structure during growth. Am Mineral 79:892-903

Rakovan J, Reeder RJ (1996) Intracrystalline rare earth element distributions in apatite: Surface structural influences on incorporation during growth. Geochim Cosmochim Acta 60:4435-4445
Rakovan J, Waychunas G (1996) Luminescence in Minerals. Mineral Rec 27:7-19
Rakovan J, McDaniel DK, Reeder RJ (1997) Use of surface-controlled REE sectoral zoning in apatite from Llallagua, Bolivia, to determine a single-crystal Sm-Nd age. Earth Planet Sci Lett 146:329-336
Rakovan J, Newville M, Sutton S (2001a) Evidence of heterovalent europium in zoned Llallagua apatite using wavelength dispersive XANES. Am Mineral 86:697-700
Rakovan J, Sutton S, Newville M (2001b) Evaluation of europium oxidation state and anomalous partitioning behavior in intrasectorally zoned apatite using wavelength dispersive micro-XANES. Advanced Photon Source, 2001 Activity Report
Rakovan J, Jaszczak JA (2002) Multiple length scale growth spirals on metamorphic graphite {001} surfaces studied by atomic force microscopy. Am Mineral 87:17-24
Reeder RJ, Grams JC (1987) Sector zoning in calcite cement crystals: Implications for trace element distributions in carbonates. Geochim Cosmochim Acta 51:187-194
Reeder RJ, Rakovan J (1999) Surface structural controls on trace element incorporation during crystal growth. *In* Growth, Dissolution and Pattern Formation in Geosystems. Jamtveit B, Meakin P (eds) Kluwer, Boston
Richards RP, Rakovan J (2000) The first occurrence of apatite crystals in Ohio. Rocks Mineral 75:255
Ringwood AE (1955) The principles governing trace element distribution during crystallization. Part I: The influence of electronegativity. Geochim Cosmochim Acta 7:189-202
Seaman JC, Arey JS, Bertsch PM (2001) Immobilization of nickel and other metals in contaminated sediments by hydroxyapatite addition. J Environ Qual 30:460-469
Sha LK, Chappell BW (1999) Apatite chemical composition, determined by electron microprobe and laser-ablation inductively coupled plasma mass spectrometry, as a probe into granite petrogenesis. Geochim Cosmochim Acta 63:3861-3881
Shtukenberg AG, Punin YO, Haegele E, Klapper H (2001) On the origin of inhomogeneity of anomalous birefringence in mixed crystals: An example of alums. Phys Chem Mineral 28:665-674
Skinner HCW (1987) Bone: Mineralization. *In* The Scientific Basis of Orthopaedics. Albright JA, Brand RA (eds) Appleton and Lange, Norwalk, Connecticut
Snoeyink VL, Jenkins D (1980) Water Chemistry. Wiley and Sons, New York
Stumm W, Morgan JJ (1996) Aquatic Chemistry. Wiley Interscience, New York
Sunagawa I, Bennema P (1982) Morphology of growth spirals: Theoretical and experimental. *In* Preparation and Properties of Solid State Materials. Wilcox WR (ed) Marcel Dekker, New York
Sunagawa I. (1984) Growth of crystals in nature. *In* Materials Science of the Earth's Interior. Sunagawa I (ed) Terra Scientific Publishing, Tokyo
Sunagawa I (1987a) Morphology of minerals. *In* Morphology of Crystals. Sunagawa I (ed) Terra Scientific Publishing, Tokyo
Sunagawa I (1987b) Surface microtopography of crystal faces. *In* Morphology of Crystals. Sunagawa I (ed) Terra Scientific Publishing, Tokyo
Teng HH, Dove PM, De Yoreo JJ (1999) Reversed calcite morphologies induced by microscopic growth kinetics: Insight into biomineralization. Geochim Cosmochim Acta 63:2507-2512
Termine JD, Peckauskas RA, Posner AS (1970) Calcium phosphate formation *in vitro*. II. Effect of environment on amorphous-crystalline transformation. Arch Biochem Biophys 140:318-325
Terpstra RA, Bennema P (1987) Crystal morphology of octacalcium phosphate: Theory and observation. J Cryst Growth 82:416-26
Terpstra RA, Bennema P, Hartman P, Woensdregt CF, Perdok WG, Senechal ML (1986) F faces of apatite and its morphology: Theory and observation. J Cryst Growth 78:468-78
Thirioux L, Baillif P, Ildefonse JP, Touray JC (1990) Surface reactions during fluorapatite dissolution-recrystallization in acid media (hydrochloric and citric acids). Geochim Cosmochim Acta 54: 1969-1977
Valsami-Jones, E., Ragnarsdottir, K.V., Putnis, A., Bosbach, D., Kemp, A.J., andCressey, G. (1998) The dissolution of apatite in the presence of aqueous metal cations at pH 2-7. Chem Geol 151: 215-233
Van Cappellen P, Berner RA (1991) Fluorapatite crystal-growth from modified seawater solutions. Geochim Cosmochim Acta 55:1219-1234
Velthuizen JV (1992) Giant fluorapatite crystals: a question of locality. Mineral Rec 23:459-463
Watson EB, Capobianco CJ (1981) Phosphorus and rare-earth elements in felsic magmas: An assessment of the role of apatite. Geochim Cosmochim Acta 45:2349-2358
Watson EB, Harrison TM (1984a) Accessory minerals and the geochemical evolution of crustal magmatic systems: A summary and prospectus of experimental approaches. Phys Earth Planet Inter 5:19-30
Watson EB, Harrison TM (1984b) What can accessory minerals tell us about felsic magma evolution? A framework for experimental study. Proc 27th Intl Geol Congr 11:503-520

Wu W, Nancollas GH (1998) The influence of additives and impurities on crystallization kinetics: An interfacial tension approach. *In* Water Soluble Polymers. Amjad Z (ed) Plenum Press, New York

Young RA, Brown WE (1982) Structures of biological minerals. *In* Biological Mineralization and Demineralization. Nancollas GH (ed) Springer-Verlag, Berlin

Zieba A, Sethuraman G, Perez F, Nancollas GH, Cameron D (1996) Influence of organic phosphonates on hydroxyapatite crystal growth kinetics. Langmuir 12:2853-2858